

This is a repository copy of *Proteasome inhibition for treatment of leishmaniasis, Chagas disease and sleeping sickness*.

White Rose Research Online URL for this paper:

<https://eprints.whiterose.ac.uk/id/eprint/105039/>

Version: Accepted Version

Article:

Khare, Shilpi, Nagle, Advait S, Biggart, Agnes et al. (32 more authors) (2016) Proteasome inhibition for treatment of leishmaniasis, Chagas disease and sleeping sickness. *Nature*. pp. 229-233. ISSN: 0028-0836

<https://doi.org/10.1038/nature19339>

Reuse

Items deposited in White Rose Research Online are protected by copyright, with all rights reserved unless indicated otherwise. They may be downloaded and/or printed for private study, or other acts as permitted by national copyright laws. The publisher or other rights holders may allow further reproduction and re-use of the full text version. This is indicated by the licence information on the White Rose Research Online record for the item.

Takedown

If you consider content in White Rose Research Online to be in breach of UK law, please notify us by emailing eprints@whiterose.ac.uk including the URL of the record and the reason for the withdrawal request.

1 Proteasome inhibition for treatment of leishmaniasis, Chagas disease and 2 sleeping sickness

3 Shilpi Khare^{1*}, Advait S. Nagle^{1*}, Agnes Biggart¹, Yin H. Lai¹, Fang Liang¹, Lauren C. Davis¹, S.
4 Whitney Barnes¹, Casey J. N. Mathison¹, Elmarie Myburgh^{2,3}, Mu-Yun Gao¹, J. Robert Gillespie⁴,
5 Xianzhong Liu¹, Jocelyn L. Tan¹, Monique Stinson¹, Ianne C. Rivera¹, Jaime Ballard¹, Vince Yeh¹, Todd
6 Groessl¹, Glenn Federe¹, Hazel X. Y. Koh⁵, John D. Venable¹, Badry Bursulaya¹, Michael Shapiro¹,
7 Pranab K. Mishra¹, Glen Spraggon¹, Ansgar Brock¹, Jeremy C. Mottram^{2,3}, Frederick S. Buckner⁴,
8 Srinivasa P. S. Rao⁵, Ben G. Wen¹, John R. Walker¹, Tove Tuntland¹, Valentina Molteni¹, Richard J.
9 Glynne¹ & Frantisek Supek¹

10 **Chagas disease, leishmaniasis, and sleeping sickness affect 20 million people worldwide and lead to**
11 **more than 50,000 deaths annually¹. The diseases are caused by infection with the kinetoplastid**
12 **parasites *Trypanosoma cruzi*, *Leishmania* spp. and *Trypanosoma brucei* spp., respectively. These**
13 **parasites have similar biology and genomic sequence, suggesting that all three diseases could be**
14 **cured with drug(s) modulating the activity of a conserved parasite target². However, no such**
15 **molecular targets or broad spectrum drugs have been identified to date. Here we describe a**
16 **selective inhibitor of the kinetoplastid proteasome (GNF6702) with unprecedented *in vivo* efficacy,**
17 **which cleared parasites from mice in all three models of infection. GNF6702 inhibits the**
18 **kinetoplastid proteasome through a non-competitive mechanism, does not inhibit the mammalian**
19 **proteasome or growth of mammalian cells, and is well-tolerated in mice. Our data provide genetic**
20 **and chemical validation of the parasite proteasome as a promising therapeutic target for treatment**
21 **of kinetoplastid infections, and underscore the possibility of developing a single class of drugs for**
22 **these neglected diseases.**

23 Kinetoplastid infections affect predominantly poor communities in Latin America, Asia and Africa.
24 Available therapies suffer from multiple shortcomings, and new drug discovery for these diseases is
25 limited by insufficient investment³. We sought low molecular weight compounds with a growth
26 inhibitory effect on *Leishmania donovani* (*L. donovani*)^{4,5}, *Trypanosoma cruzi* (*T. cruzi*)^{6,7} and
27 *Trypanosoma brucei* (*T. brucei*)^{5,8}. Our approach was to test 3 million compounds in proliferation assays
28 on all three parasites (Supplementary Information Tables 1-3), followed by triaging of active compounds
29 (half-maximum inhibitory concentration value EC₅₀<10 μM) to select those with a clear window of
30 selectivity (>5-fold) with respect to growth inhibition of mammalian cells. An azabenzoxazole,
31 GNF5343, was identified as a hit in the *L. donovani* and *T. brucei* screens. Although GNF5343 was not
32 identified in the *T. cruzi* screen, we noted potent anti-*T. cruzi* activity of this compound in secondary
33 assays.

34 Optimization of GNF5343 involved the design and synthesis of ~3,000 compounds, and focused on
35 improving bioavailability and potency on inhibition of *L. donovani* growth within macrophages (Fig. 1).
36 A critical modification involved replacement of the azabenzoxazole center with C6-substituted imidazo-
37 and triazolopyrimidine cores, which yielded compounds up to 20-fold more potent on intra-macrophage
38 *L. donovani* (e.g. GNF2636). Replacement of the furan group with a dimethyloxazole ring reduced the
39 risk of toxicity associated with the furan moiety, and replacement of the chlorophenyl group with a
40 fluorophenyl improved selectivity over mammalian cell growth inhibition (e.g. GNF3849). These
41 changes also resulted in low clearance and acceptable bioavailability. Further substitutions at the core C6
42 position led to GNF6702 and a 400-fold increase in intra-macrophage *L. donovani* potency compared to
43 GNF5343.

44 *L. donovani* parasites cause a majority of visceral leishmaniasis (VL) cases in East Africa and India⁹. In
45 mice infected with *L. donovani*¹⁰, oral dosing with GNF6702 effected a more pronounced reduction in

liver parasite burden than miltefosine, the only oral anti-leishmanial drug available in clinical practice⁵ (Fig. 2a). The miltefosine regimen for VL efficacy studies was chosen to approximate the drug plasma concentration of the clinical regimen¹¹. We noted a greater than three log reduction in parasite load after eight day treatment with 10 mg/kg of GNF6702 twice-daily with the free concentration of GNF6702 (fraction unbound in plasma=0.063) staying above the *L. donovani* EC₉₉ value (the concentration inhibiting 99% of intra-macrophage parasite growth *in vitro*) for the duration of the dosing period (Extended Data Fig. 1a). Characterization of efficacy of ten analogues in the series at various doses revealed a significant correlation ($r^2=0.89$, $p<0.01$) between i) the ratio of mean free plasma compound concentration to the *L. donovani* EC₉₀ value and ii) reduction of the liver parasite burden. We found that 90% parasite burden reduction in the mouse model was achieved when the mean free compound plasma concentration during treatment equaled a 0.94-fold multiple of the *L. donovani* EC₉₀ value (Fig. 2b). Cutaneous leishmaniasis (CL) affects about a million people per year, causing skin lesions that can resolve into scar tissue¹². In parts of the Middle East, CL has reached epidemic proportions¹³. After footpad infection of BALB/c mice with the dermatotropic *L. major* strain^{14,15}, treatment with GNF6702 at 10 mg/kg twice-daily caused a 5-fold decrease in footpad parasite burden and a reduction in footpad swelling (Fig. 2c). Both 3 mg/kg and 10 mg/kg twice-daily regimens of GNF6702 were superior to 30 mg/kg once-daily miltefosine regimen ($p<0.01$), which translates into ~2-fold higher miltefosine plasma concentration in mice than observed in clinical dosing¹¹. We further tested if GNF6702 can cure additional kinetoplastid parasite infections. An estimated 25% of the 8 million people infected with *T. cruzi* will develop chronic Chagas disease, manifesting as cardiac or intestinal dysfunction^{16,17}. Benznidazole is broadly used for treatment of acute and indeterminate stages of Chagas disease in Latin America^{18,19}. However, benznidazole has side-effects that frequently lead to treatment interruption^{18,20-22} and a better tolerated drug is needed. To model treatment in the

69 indeterminate disease stage, we infected mice with *T. cruzi* parasites and began treatment 35 days after
70 infection, when the immune system of the mice had controlled parasite burden²³. We increased the
71 parasite detection sensitivity by immunosuppressing the mice after 20 days of treatment^{23,24}. In this
72 model, GNF6702 dosed twice-daily at 10 mg/kg matched the efficacy of benznidazole at 100 mg/kg
73 once-daily; all but one treated mice had no detectable parasites in blood, colon or heart tissue, even after
74 4 weeks of immunosuppression (Fig. 2d).

75 Finally, we tested GNF6702 in a mouse model of stage II sleeping sickness (human African
76 trypanosomiasis - HAT)²⁵. Mortality of stage II HAT is caused by infection of the CNS and, in this
77 mouse model, luciferase-expressing *T. brucei* parasites establish a CNS infection by day 21 post-
78 infection. GNF6702 was administered at 100 mg/kg once-daily to account for low exposure in the brain
79 relative to the plasma (~10%, Extended Data Fig. 1b). Diminazene aceturate, a stage I drug that poorly
80 crosses the blood-brain barrier, effected apparent clearance of parasites from the blood after a single dose,
81 but did not prevent parasite recrudescence 21 days later. By contrast, treatment with GNF6702 for seven
82 days caused a sustained clearance of parasites (days 42 and 92 post-infection in Fig. 2e, Extended Data
83 Fig. 2a, Supplementary Information Tables 4 and 5). Significantly, mice treated with GNF6702 had no
84 detectable parasites in the brain at termination of the experiment, though parasites were clearly detected
85 in the brains of mice treated with diminazene aceturate (Extended Data Fig. 2b, Supplementary
86 Information Table 6).

87 As GNF6702 showed compelling efficacy in four mouse models of kinetoplastid infections: VL, CL,
88 Chagas disease and stage II HAT, we reasoned that mechanistic studies of GNF6702 might identify a
89 pan-kinetoplastid drug target that could inform target-based drug discovery efforts. We attempted to
90 evolve *L. donovani* strains resistant to GNF3943 and GNF8000 (early analogues from the series,
91 Extended Data Fig. 3) through 12 months of parasite culture under drug pressure without success.

92 However, we were able to select two drug-resistant *T. cruzi* epimastigote isolates, one resistant to
 93 GNF3943, and another to GNF8000. Both *T. cruzi* lines exhibited at least 40-fold lower susceptibility to
 94 GNF6702 than wild type *T. cruzi* (Extended Data Fig. 4a and 4b). Using whole genome sequencing, we
 95 found that the GNF3943-resistant line had a homozygous mutation encoding a substitution of isoleucine
 96 for methionine at amino acid 29 in the proteasome beta 4 subunit (*PSMB4*^{I29M/I29M}) and a heterozygous
 97 mutation P82L in dynein heavy chain gene. The GNF8000-resistant line had a heterozygous F24L
 98 mutation in *PSMB4*, and four other heterozygous mutations (Extended Data Table 1). We focused our
 99 attention on the proteasome as a likely target for the compound series because we found two independent
 100 mutations in the *PSMB4* gene, and because the proteasome is an essential enzyme in eukaryotic cells. We
 101 also note that the *Plasmodium falciparum* proteasome has recently been the target of promising drug
 102 discovery efforts for malaria²⁶.
 103 We first asked whether two prototypic inhibitors of mammalian proteasome, bortezomib and MG132,
 104 could also block *T. cruzi* growth. Indeed, both compounds inhibited *T. cruzi* epimastigote proliferation
 105 with sub-micromolar potency. However, in contrast to GNF6702, bortezomib and MG132 inhibited
 106 proliferation of the two resistant lines (*PSMB4*^{I29M/I29M}, *PSMB4*^{wt/F24L}) with comparable potency to the
 107 wild type parasites. Additionally, the *PSMB4* mutant lines were not resistant to nifurtimox, an anti-
 108 kinetoplastid drug with an unrelated mechanism of action (Extended Data Fig. 4a and 4b). To determine
 109 whether the F24L mutation was sufficient to confer resistance to GNF6702, we engineered *T. cruzi*
 110 epimastigote lines that ectopically expressed either wild type or F24L-mutated PSMB4. Overexpression
 111 of *PSMB4*^{WT} had little effect on the EC₅₀ value for GNF6702, whereas overexpression of *PSMB4*^{F24L}
 112 caused a greater than 10-fold reduction in GNF6702 potency, but not in that of bortezomib (Fig. 3a,
 113 Extended Data Fig. 4c). Previously, bortezomib was also shown to inhibit the growth of *T. brucei*,
 114 suggesting that proteasome activity is essential for growth in this parasite as well²⁷. To test whether

115 PSMB4^{F24L} can rescue growth inhibition by GNF6702 in *T. brucei*, we engineered two parasite strains
116 that ectopically expressed wild type and F24L-mutated PSMB4, respectively. Similar to *T. cruzi*,
117 overexpression of PSMB4^{F24L} in *T. brucei* conferred a high level of resistance to GNF6702 (~70-fold
118 shift in EC₅₀ value), while having no effect on parasite susceptibility to bortezomib (Fig. 3b, Extended
119 Data Fig. 4c).

120 We next asked whether GNF6702 could inhibit any of three *T. cruzi* proteasome proteolytic activities in
121 biochemical assays. As predicted from the *T. cruzi* genome²⁸, mass spectrometry analysis of purified *T.*
122 *cruzi* proteasome identified seven alpha and seven beta proteasome subunits, including PSMB4
123 (Supplementary Tables 7 and 8). Using substrates that are specific for each of the chymotrypsin-like,
124 trypsin-like and caspase-like proteolytic activities, we found that only the chymotrypsin-like activity of
125 the *T. cruzi* proteasome was inhibited by GNF6702 (IC₅₀=35 nM), while the other two activities were not
126 affected (IC₅₀>10 μM). In contrast, bortezomib inhibited the chymotrypsin-like (IC₅₀=91 nM), the
127 caspase-like (IC₅₀=370 nM) and the trypsin-like (IC₅₀=1.7 μM) activities. We further found that the
128 chymotrypsin-like activity of the PSMB4^{I29M} *T. cruzi* proteasome was at least 300-fold less susceptible to
129 GNF6702 (IC₅₀>10 μM) and ~3-fold less susceptible to bortezomib (IC₅₀=0.26 μM), while susceptibility
130 of the other two mutant proteasome proteolytic activities to the two inhibitors were not affected (Fig. 4a,
131 Extended Data Table 2).

132 We reasoned that if the primary mechanism of parasite growth inhibition by the compound series was
133 through inhibition of the proteasome chymotrypsin-like activity, then the IC₅₀ values for this proteolytic
134 activity should correlate with EC₅₀ values for parasite proliferation. Indeed, a tight correlation between
135 the two parameters was observed for *L. donovani* axenic amastigotes and *T. brucei* bloodstream form
136 trypomastigotes (r²=0.78 and r²=0.67, respectively) over a 2,000-fold potency range for 317 analogues,
137 thus indicating that inhibition of parasite proteasome activity was driving the anti-parasitic activity of

138 these compounds. We observed a weaker correlation between IC₅₀ and EC₅₀ values for intracellular
139 *T. cruzi* ($r^2=0.36$, $p<0.01$), perhaps reflecting more complex cellular pharmacokinetics resulting from
140 compounds having to access *T. cruzi* parasites within the cytosol of mammalian cells (Fig. 4b, Extended
141 Data Fig. 5).

142 Both resistant *T. cruzi* lines retained sensitivity to bortezomib, which is a substrate-competitive inhibitor,
143 suggesting that GNF6702 might have an alternative mode of inhibition. A Lineweaver-Burk plot of
144 chymotrypsin-like activity at increasing concentrations of peptide substrate showed that GNF6702 has a
145 non-competitive mode of inhibition clearly distinct from the competitive mechanism described for
146 MG132 and bortezomib^{29,30}. We were also able to extend these observations to proteasome from *L.*
147 *donovani* (Fig. 4c, Extended Data Table 3). We further note that GNF6702 had no measurable activity on
148 the human proteasome (Fig. 4d, Extended Data Table 2). Interestingly, human proteasome beta 4 subunit
149 has a methionine at the 29th amino acid position, mirroring the I29M mutation in the GNF3943-resistant
150 *T. cruzi* line (Extended Data Fig. 6a).

151 In summary, GNF6702 blocks the chymotrypsin-like activity harbored by the beta 5 subunit without
152 competing with substrate binding, and mutations in the beta 4 subunit, which is in direct physical contact
153 with the beta 5 subunit, confer resistance to this inhibition. Next we used homology modeling of the *T.*
154 *cruzi* proteasome to look for evidence of an allosteric inhibitor binding site. In the *T. cruzi* proteasome
155 model, the F24 and I29 beta 4 residues are positioned at the interface between the beta 4 and beta 5
156 subunits, on the outer limit of the beta 5 active site. Adjacent to these two beta 4 residues and the beta 5
157 active site is a plausible binding pocket for GNF6702 (Extended Data Fig. 6b and 6c).

158 Finally, we tested whether GNF6702 can inhibit proteasome activity in intact *T. cruzi* cells. Cellular
159 proteins entering the proteasome degradation pathway are first tagged with ubiquitin, and proteasome
160 inhibition results in intracellular accumulation of ubiquitylated proteins. Treatment of *T. cruzi*

161 epimastigotes with GNF6702 led to significant buildup of ubiquitylated proteins (Extended Data Fig. 7a)
162 with the half-maximal effect (EC_{50}) achieved at 130 nM compound concentration (Extended Data Fig.
163 7c). This EC_{50} value correlated well with the half-maximal growth inhibitory concentration of GNF6702
164 on *T. cruzi* epimastigotes (EC_{50} =150 nM; Extended Data Fig. 4b). For comparison, similar experiments
165 with bortezomib yielded comparable inhibitor potencies in the two *T. cruzi* assays (ubiquitylation
166 EC_{50} =62 nM vs growth inhibition EC_{50} =160 nM; Extended Data Fig. 4b and 7c). We did not observe any
167 detectable accumulation of ubiquitylated proteins in mammalian 3T3 cells treated with GNF6702
168 (Extended Data Fig. 7b and 7c), further confirming high selectivity of this compound.

169 Validation of the parasite proteasome as the target of GNF6702 is supported through several lines of
170 evidence: i) point mutations in the *PSMB4* gene are sufficient to confer resistance to biochemical
171 proteasome inhibition and cellular *T. cruzi* growth inhibition; ii) GNF6702 is a selective inhibitor of
172 parasite proteasome activity and does not inhibit the human proteasome, mirroring the selective
173 inhibition of parasite growth over mammalian cell growth; and iii) potency of GNF6702 and analogues in
174 parasite proteasome assays predict potency in parasite growth inhibition assays.

175 In this work we show that in mouse disease models, GNF6702 was able to eradicate parasites from
176 diverse niches that included the cytosol (*T. cruzi*), phagolysosome (*L. donovani*, *L. major*) of infected
177 host cells, and brain (*T. brucei*). GNF6702 has also good pharmacokinetic properties, and the compound
178 did not show activity in panels of human receptor, enzyme and ion channel assays (Supplementary
179 Tables 9-11). Going forward, GNF6702, or analogues thereof, has potential to yield a new treatment for
180 several kinetoplastid infections and it is currently being evaluated in preclinical toxicity studies. It is
181 unclear if the clinical utility of GNF6702 could extend to the treatment of stage II HAT as GNF6702 was
182 tested in the HAT mouse model only at one high dose (100 mg/kg once-daily). We also note that
183 identification of a broadly active pan-kinetoplastid drug might not be feasible (or desirable) as such a

184 drug would need to reach high concentrations in varied tissues/subcellular compartments, and might
185 carry increased toxicity risk. Instead, alternative analogues from this series with different
186 pharmacological profiles might be needed for treatment of different kinetoplastid infections. Nevertheless,
187 there are only scarce resources for drug development in these diseases, and identification of a common
188 target and chemical scaffold with potential across multiple indications provides new hope for improved
189 treatment options for some of the world's poorest people.

190 REFERENCES

- 191 1. Research priorities for Chagas disease, human African trypanosomiasis and leishmaniasis. *World*
192 *Health Organization, WHO Technical Report Series* 975, 1-100 (2012).
- 193 2. El-Sayed, N. M. *et al.* Comparative genomics of trypanosomatid parasitic protozoa. *Science* 309, 404-
194 409, doi:10.1126/science.1112181 (2005).
- 195 3. Bilbe, G. Infectious diseases. Overcoming neglect of kinetoplastid diseases. *Science* 348, 974-976,
196 doi:10.1126/science.aaa3683 (2015).
- 197 4. Sundar, S. & Chakravarty, J. An update on pharmacotherapy for leishmaniasis. *Expert Opinion on*
198 *Pharmacotherapy* 16, 237-252, doi:10.1517/14656566.2015.973850 (2015).
- 199 5. Nagle, A. S. *et al.* Recent developments in drug discovery for leishmaniasis and human African
200 trypanosomiasis. *Chemical Reviews*, doi:10.1021/cr500365f (2014).
- 201 6. Bern, C. Chagas' Disease. *The New England Journal of Medicine* 373, 456-466,
202 doi:10.1056/NEJMr1410150 (2015).
- 203 7. Chatelain, E. Chagas disease drug discovery: toward a new era. *Journal of Biomolecular Screening*
204 20, 22-35, doi:10.1177/1087057114550585 (2015).

- 205 8. Kennedy, P. G. Clinical features, diagnosis, and treatment of human African trypanosomiasis
206 (sleeping sickness). *The Lancet. Neurology* 12, 186-194, doi:10.1016/S1474-4422(12)70296-X
207 (2013).
- 208 9. Control of the leishmaniasis. *World Health Organization, WHO Technical Report Series* 949, 37-39
209 (2010).
- 210 10. Yardley, V. & Croft, S. L. A comparison of the activities of three amphotericin B lipid formulations
211 against experimental visceral and cutaneous leishmaniasis. *International Journal of Antimicrobial*
212 *Agents* 13, 243-248 (2000).
- 213 11. Dorlo, T. P. *et al.* Pharmacokinetics of miltefosine in Old World cutaneous leishmaniasis patients.
214 *Antimicrobial Agents and Chemotherapy* 52, 2855-2860, doi:10.1128/AAC.00014-08 (2008).
- 215 12. McGwire, B. S. & Satoskar, A. R. Leishmaniasis: clinical syndromes and treatment. *QJM : Monthly*
216 *journal of the Association of Physicians* 107, 7-14, doi:10.1093/qjmed/hct116 (2014).
- 217 13. Hotez, P. J. Combating the next lethal epidemic. *Science* 348, 296-297,
218 doi:10.1126/science.348.6232.296-b (2015).
- 219 14. Sacks, D. & Anderson, C. Re-examination of the immunosuppressive mechanisms mediating non-
220 cure of *Leishmania* infection in mice. *Immunological Reviews* 201, 225-238, doi:10.1111/j.0105-
221 2896.2004.00185.x (2004).
- 222 15. Nelson, K. G., Bishop, J. V., Ryan, R. O. & Titus, R. Nanodisk-associated amphotericin B clears
223 *Leishmania major* cutaneous infection in susceptible BALB/c mice. *Antimicrobial Agents and*
224 *Chemotherapy* 50, 1238-1244, doi:10.1128/AAC.50.4.1238-1244.2006 (2006).
- 225 16. Nunes, M. C. *et al.* Chagas disease: an overview of clinical and epidemiological aspects. *Journal of*
226 *the American College of Cardiology* 62, 767-776, doi:10.1016/j.jacc.2013.05.046 (2013).

227 17. Coura, J. R. & Borges-Pereira, J. Chagas disease: 100 years after its discovery. A systemic review.
 228 *Acta Tropica* 115, 5-13, doi:10.1016/j.actatropica.2010.03.008 (2010).

229 18. Bern, C. Antitrypanosomal therapy for chronic Chagas' disease. *The New England Journal of*
 230 *Medicine* 364, 2527-2534, doi:10.1056/NEJMct1014204 (2011).

231 19. Viotti, R. *et al.* Towards a paradigm shift in the treatment of chronic Chagas disease. *Antimicrobial*
 232 *Agents and Chemotherapy* 58, 635-639, doi:10.1128/AAC.01662-13 (2014).

233 20. Molina, I. *et al.* Randomized trial of posaconazole and benznidazole for chronic Chagas' disease. *The*
 234 *New England Journal of Medicine* 370, 1899-1908, doi:10.1056/NEJMoa1313122 (2014).

235 21. Morillo, C. A. *et al.* Randomized trial of benznidazole for chronic Chagas' cardiomyopathy. *The New*
 236 *England Journal of Medicine* 373, 1295-1306, doi:10.1056/NEJMoa1507574 (2015).

237 22. Viotti, R. *et al.* Side effects of benznidazole as treatment in chronic Chagas disease: fears and
 238 realities. *Expert Review of Anti-Infective Therapy* 7, 157-163, doi:10.1586/14787210.7.2.157 (2009).

239 23. Khare, S. *et al.* Antitrypanosomal treatment with benznidazole is superior to posaconazole regimens
 240 in mouse models of Chagas disease. *Antimicrobial Agents and Chemotherapy* 59, 6385-6394,
 241 doi:10.1128/AAC.00689-15 (2015).

242 24. Bustamante, J. M., Bixby, L. M. & Tarleton, R. L. Drug-induced cure drives conversion to a stable
 243 and protective CD8+ T central memory response in chronic Chagas disease. *Nature Medicine* 14,
 244 542-550, doi:10.1038/nm1744 (2008).

245 25. Myburgh, E. *et al.* In vivo imaging of trypanosome-brain interactions and development of a rapid
 246 screening test for drugs against CNS stage trypanosomiasis. *PLoS Neglected Tropical Diseases* 7,
 247 e2384, doi:10.1371/journal.pntd.0002384 (2013).

248 26. Li, H. *et al.* Structure- and function-based design of *Plasmodium*-selective proteasome inhibitors.
 249 *Nature* 530, 233-236, doi:10.1038/nature16936 (2016).

250 27. Steverding, D. & Wang, X. Trypanocidal activity of the proteasome inhibitor and anti-cancer drug
251 bortezomib. *Parasites & Vectors* 2, 29, doi:10.1186/1756-3305-2-29 (2009).

252 28. Ivens, A. C. *et al.* The genome of the kinetoplastid parasite, *Leishmania major*. *Science* 309, 436-442,
253 doi:10.1126/science.1112680 (2005).

254 29. Li, X. *et al.* Effect of noncompetitive proteasome inhibition on bortezomib resistance. *Journal of the*
255 *National Cancer Institute* 102, 1069-1082, doi:10.1093/jnci/djq198 (2010).

256 30. Fernandez, Y. *et al.* Chemical blockage of the proteasome inhibitory function of bortezomib: impact
257 on tumor cell death. *The Journal of Biological Chemistry* 281, 1107-1118,
258 doi:10.1074/jbc.M511607200 (2006).

259 **References to the Methods section**

260 31. Zhang, X., Goncalves, R. & Mosser, D. M. The isolation and characterization of murine
261 macrophages. *Curr. Protoc. Immunol.* Chapter 14, Unit1 4.1 (2008).

262 32. Khare, S. *et al.* Utilizing chemical genomics to identify cytochrome b as a novel drug target for
263 Chagas disease. *PLoS Pathogens* 11, e1005058, doi:10.1371/journal.ppat.1005058 (2015).

264 33. Buckner, F. S., Verlinde, C. L., La Flamme, A. C. & Van Voorhis, W. C. Efficient technique for
265 screening drugs for activity against *Trypanosoma cruzi* using parasites expressing beta-galactosidase.
266 *Antimicrobial Agents and Chemotherapy* 40, 2592-2597 (1996).

267 34. Logan-Klumpler, F. J. *et al.* GeneDB--an annotation database for pathogens. *Nucleic Acids Research*
268 40, D98-108, doi:10.1093/nar/gkr1032 (2012).

269 35. Taylor, M. C. & Kelly, J. M. pTcINDEX: a stable tetracycline-regulated expression vector for
270 *Trypanosoma cruzi*. *BMC Biotechnology* 6, 32, doi:10.1186/1472-6750-6-32 (2006).

- 271 36. Hariharan, S., Ajioka, J. & Swindle, J. Stable transformation of *Trypanosoma cruzi*: inactivation of
272 the PUB12.5 polyubiquitin gene by targeted gene disruption. *Molecular and Biochemical*
273 *Parasitology* 57, 15-30 (1993).
- 274 37. Wirtz, E., Leal, S., Ochatt, C. & Cross, G. A. A tightly regulated inducible expression system for
275 conditional gene knock-outs and dominant-negative genetics in *Trypanosoma brucei*. *Molecular and*
276 *Biochemical Parasitology* 99, 89-101 (1999).
- 277 38. Wilk, S. & Chen, W.-E. Purification of the eukaryotic 20S proteasome. *Curr. Protoc. Protein Sci.*
278 Chapter 21 (2001).
- 279 39. Unno, M. *et al.* The structure of the mammalian 20S proteasome at 2.75 Å resolution. *Structure* 10,
280 609-618 (2002).
- 281 40. Melnick, J. S. *et al.* An efficient rapid system for profiling the cellular activities of molecular
282 libraries. *Proceedings of the National Academy of Sciences of the United States of America* 103,
283 3153-3158, doi:10.1073/pnas.0511292103 (2006).
- 284 41. Waters, N. J., Jones, R., Williams, G. & Sohal, B. Validation of a rapid equilibrium dialysis approach
285 for the measurement of plasma protein binding. *Journal of Pharmaceutical Sciences* 97, 4586-4595,
286 doi:10.1002/jps.21317 (2008).
- 287 42. Wang, J. & Skolnik, S. Recent advances in physicochemical and ADMET profiling in drug
288 discovery. *Chemistry & Biodiversity* 6, 1887-1899, doi:10.1002/cbdv.200900117 (2009).
- 289 43. Kalvass, J. C., Tess, D. A., Giragossian, C., Linhares, M. C. & Maurer, T. S. Influence of microsomal
290 concentration on apparent intrinsic clearance: implications for scaling in vitro data. *Drug Metabolism*
291 *and Disposition: the Biological Fate of Chemicals* 29, 1332-1336 (2001).

- 292 44. Li, C. *et al.* A modern in vivo pharmacokinetic paradigm: combining snapshot, rapid and full PK
293 approaches to optimize and expedite early drug discovery. *Drug Discovery Today* 18, 71-78,
294 doi:10.1016/j.drudis.2012.09.004 (2013).
- 295 45. Sacks, D. L. & Melby, P. C. Animal models for the analysis of immune responses to leishmaniasis.
296 *Curr. Protoc. Immunol.* Chapter 19, Unit 19.12 (2001).
- 297 46. McLatchie, A. P. *et al.* Highly sensitive in vivo imaging of *Trypanosoma brucei* expressing "red-
298 shifted" luciferase. *PLoS Neglected Tropical Diseases* 7, e2571, doi:10.1371/journal.pntd.0002571
299 (2013).

300 FIGURE LEGENDS

301 **Figure 1: Chemical evolution of GNF6702 from the phenotypic hit GNF5343.** *L. donovani*:
302 amastigotes proliferating within primary mouse macrophages; *T. brucei*: the bloodstream form
303 trypomastigotes; *T. cruzi*: amastigotes proliferating in 3T3 fibroblast cells; macrophage: mouse primary
304 peritoneal macrophages; EC₅₀ and CC₅₀: half-maximum growth inhibition concentration; F: oral
305 bioavailability in mouse after administering single compound dose (20 mg/kg) as a suspension; CL:
306 plasma clearance in mouse after single iv bolus dose (5 mg/kg); N.D.: not determined; all EC₅₀ and CC₅₀
307 values correspond to means \pm s.e.m. (n=4 technical replicates).

308 **Figure 2: GNF6702 clears parasites in mouse models of kinetoplastid infections.** **a**, Post-treatment *L.*
309 *donovani* liver burdens in mouse model of VL as assessed by qPCR (n=5 mice). **b**, PK/PD relationship
310 for ten GNF6702 analogues, each administered at several doses; circles: mean liver burdens associated
311 with individual compound regimens (30 regimens in total; n=5 mice per regimen) relative to vehicle;
312 horizontal dotted line: 90% reduction in the liver *L. donovani* burden; vertical dotted line: 0.94-fold
313 multiple of the mean free compound plasma concentration/ the *L. donovani* EC₉₀ value ratio. **c**, Post-
314 treatment *L. major* footpad burdens in the BALB/c mouse model of CL as assessed by qPCR (n= 6 mice);

the p values (two-tailed distribution) relate parasite burdens in compound-treated mice with those from vehicle-treated mice; left inset picture: a representative mouse footpad after treatment with vehicle; right inset picture: a representative mouse footpad after treatment with GNF6702 10 mg/kg twice-daily regimen. **d**, *T. cruzi* burden in mouse blood (circles), colon (triangles) and heart (diamonds) as assessed by qPCR after 20 days of treatment and four weeks of immunosuppression (n=8 mice). **e**, Whole body *in vivo* imaging of bioluminescent *T. brucei* before and after treatment; *Trypanosoma brucei*-infected mice were treated by a single intraperitoneal injection of diminazene aceturate (n=3 mice) or by oral administration of GNF6702 once-daily for 7 days (n=6 mice); filled symbols show whole body bioluminescence values for individual mice; several mice from the untreated and diminazene aceturate-treated groups were euthanized between days 28 and 56 due to CNS infection symptoms; background bioluminescence values shown for uninfected mice (grey-filled squares; n=4) were collected independently from mice aged-matched for day 0 using the same acquisition settings. Red dotted lines in **a**, **c** and **d** plots show limit of parasite detection by qPCR; plot symbols below the red dotted line: mice with no detectable parasites; data points below the limit of detection are 'jittered' to show number of animals in a group; thick horizontal lines: means of the treatment groups; RU: relative units (parasite burden relative to the mean burden of the vehicle-treated group).

Figure 3: F24L mutation in proteasome beta 4 subunit confers selective resistance to GNF6702. a, growth inhibition of *T. cruzi* epimastigote strains ectopically expressing PSMB4^{WT} or PSMB4^{F24L} protein by GNF6702 and bortezomib; non-induced/induced: culture medium without/with tetracycline to modulate expression of tetracycline-inducible *PSMB4* genes. **b**, growth inhibition of *T. brucei* bloodstream form trypomastigotes constitutively overexpressing PSMB4^{WT} or PSMB4^{F24L} protein by GNF6702 and bortezomib. EC₅₀ values for each strain/compound pair are listed inside **a** and **b** plot panels next to corresponding strain/compound symbol (defined in plot legends); means from n=3

technical replicates are shown; error bars represent s.e.m. values; for data points lacking error bars, s.e.m. values are smaller than circles representing means; due to limited aqueous solubility, the highest tested GNF6702 concentration was 10 μ M. RU (relative units) in **a** and **b** corresponds to parasite growth relative to the DMSO control (%).

Figure 4: Compounds from GNF6702 series inhibit growth of kinetoplastid parasites by inhibiting parasite proteasome chymotrypsin-like activity. **a**, Inhibition of three proteolytic activities of purified wild type (PSMB4^{WT}) and PSMB4^{I29M} *T. cruzi* proteasomes by GNF6702 and bortezomib; IC₅₀ values for proteasome proteolytic activities are listed inside plots. **b**, Correlation between inhibition of chymotrypsin-like activity of purified *L. donovani* proteasome (IC₅₀) and *L. donovani* axenic amastigote growth inhibition (EC₅₀; data points correspond to means of 2 technical replicates); red circles: IC₅₀>20 μ M; blue circles: EC₅₀>25 μ M; yellow circles: IC₅₀>20 μ M and EC₅₀>25 μ M; data for 317 analogues are shown. **c**, Lineweaver-Burk plot of inhibition of *T. cruzi* proteasome chymotrypsin-like activity by GNF6702 at increasing concentrations of a peptide substrate. **d**, Effect of GNF6702 and bortezomib on three proteolytic activities of human constitutive proteasome; IC₅₀ values for proteasome proteolytic activities are listed inside plots. Data shown in **a**, **c** and **d** represent means \pm s.e.m. (n=3 technical replicates; for data points lacking error bars, s.e.m. values are smaller than circles representing means). Due to limited aqueous solubility, the highest tested GNF6702 concentration in experiments shown in **a** and **d** was 10 μ M.

METHODS

Ethics statement for animal models. All procedures involving mice were performed in accordance with AAALAC standards or under UK Home Office regulations, and were reviewed and approved in accordance with the Novartis Animal Welfare Policy. Sample size was determined on the basis of the

minimum number of animals required for good data distribution and statistics. Blinding was not possible in these experiments but animals were selected randomly for each group.

Determination of IC₅₀, EC₅₀ and CC₅₀ values, and data correlation. Reported IC₅₀/ EC₅₀/ CC₅₀ values were calculated by averaging IC₅₀/ EC₅₀/ CC₅₀ values obtained from individual technical replicate experiments (n; specified in relevant Figure captions and Methods sub-sections). Each technical replicate experiment was performed on a different day with freshly prepared reagents. Reported standard errors of mean (s.e.m.) were calculated using IC₅₀/ EC₅₀/ CC₅₀ values determined in individual technical replicate experiments. To calculate IC₅₀/ EC₅₀/ CC₅₀ values, measured dose response values were fitted with 4-parameter logistic function $y=A+(B-A)/(1+(x/C)^D)$ (model 201, XLfit, IDBS), where x refers to compound concentration and y corresponds to an assay readout value.

VL efficacy data for ten GNF6702 analogues (Fig. 2a) were fitted with 4-parameter logistic function $y=A+(B-A)/(1+(x/C)^D)$ (model 201, XLfit, IDBS), where x values correspond to free mean compound plasma concentrations and y values correspond to $\log_{10}(L. donovani$ liver burden).

To correlate parasite proteasome inhibition with parasite growth inhibition (Fig. 4b and Extended data Fig. 5), we fitted data with $y=a*x+b$ function using the least square method (x corresponds to $\log_{10}(\text{IC}_{50})$; y corresponds to $\log_{10}(\text{EC}_{50})$).

***Leishmania donovani* axenic amastigote growth inhibition assay.** RPMI 1640 medium (HyClone) was supplemented with 20% heat-inactivated fetal bovine serum (Omega Scientific), 23 μM folic acid (Sigma-Aldrich), 100 μM adenosine (Sigma-Aldrich), 22 mM D-glucose (Sigma-Aldrich), 4 mM L-glutamine (Hyclone), 25 mM 2-(4-morpholino) ethanesulfonic acid (Sigma-Aldrich) and 100 IU penicillin/ 100 $\mu\text{g/mL}$ streptomycin (HyClone), and adjusted to pH= 5.5 with 6 M hydrochloric acid (Fisher Scientific) at 37 °C. *Leishmania donovani* MHOM/SD/62/1S-CL2D axenic amastigotes were

382 cultured in 10 mL of this medium (Axenic Amastigote Medium) in T75 CELL-STAR flasks (Greiner
383 Bio-One) at 37 °C/ 5% CO₂ and passaged once a week.

384 To determine compound growth inhibitory potency on *L. donovani* axenic amastigotes, 100 nL of serially
385 diluted compounds in DMSO were transferred to the wells of white, solid bottom 384-well plates
386 (Greiner Bio-One) by Echo 555 acoustic liquid handling system (Labcyte). Then, 1 x 10³ of *L. donovani*
387 axenic amastigotes in 40 µL of Axenic Amastigote Medium were added to each well, and plates were
388 incubated for 48 hours at 37 °C/ 5% CO₂. Parasite numbers in individual plate wells were determined
389 through quantification of intracellular ATP. The CellTiter-Glo luminescent cell viability reagent
390 (Promega) was added to plate wells, and ATP-dependent luminescence signal was measured on an
391 EnVision MultiLabel Plate Reader (Perkin Elmer). Luminescence values in wells with compounds were
392 divided by the average luminescence value of the plate DMSO controls, and used for calculation of
393 compound EC₅₀ values as described above.

394 Axenic amastigote EC₅₀ values shown in Fig. 4b correspond to means of 2 technical replicates.

395 **Isolation and maintenance of *Leishmania donovani* splenic amastigotes.** Female BALB/cJ mice
396 (Envigo) infected with *L. donovani* MHOM/ET/67/HU3 (ATCC) for 50-80 days were euthanized, and
397 infected spleens were removed and weighed. The weight of an infected spleen ranged from 300 to 600
398 mg. For comparison, spleens from non-infected age-matched BALB/cJ mice weighed ~100 mg. Infected
399 spleens were washed in Axenic Amastigote Medium (composition described above) and placed into
400 Falcon 50 mL conical centrifuge tubes (Fisher Scientific) containing ice-cold Axenic Amastigote
401 Medium (15 mL per infected spleen). Spleens were homogenized on ice in a Dounce homogenizer and
402 centrifuged at 200 x g for 15 minutes at 4 °C to remove tissue debris. *Leishmania donovani* amastigotes
403 present in the supernatant were pelleted by centrifugation at 1,750 x g for 15 min at 4 °C and re-
404 suspended either in Axenic Amastigote Medium (when used for *in vitro* macrophage infections) or in

Hanks' Balanced Salt Solution (when used for mouse infections; Hyclone). Suspensions of splenic amastigotes were kept on ice and used for *in vitro* or *in vivo* infections within 2-3 hours. To propagate *L. donovani* amastigotes *in vivo*, 6 to 7 weeks old female BALB/cJ mice were infected with 8×10^7 purified splenic amastigotes in 200 μ L of Hanks' Balanced Salt Solution by tail vein injection.

***Leishmania donovani* intra-macrophage amastigote growth inhibition assay.** *In vitro* compound potencies on intra-macrophage *L. donovani* MHOM/ET/67/HU3 were determined using primary murine peritoneal macrophages infected with *L. donovani* splenic amastigotes. Primary macrophages were elicited in female BALB/c mice for 72 hours following the injection of 500 μ L of sterile aqueous 2% starch (J. T. Baker) solution into the mouse peritoneal cavity. The protocol used for isolation of peritoneal macrophages was described in detail previously³¹. The isolated macrophages were re-suspended in Macrophage Infection Medium (RPMI-1640 medium supplemented with 2 mM L-glutamine, 10% heat-inactivated fetal bovine serum, 10 mM sodium pyruvate (Hyclone), and 100 IU penicillin/ 100 μ g/mL streptomycin), and 50 μ L of macrophage suspension (8×10^5 macrophages/mL) were added to microscopy-grade, clear-bottom, black 384-well plates (Greiner Bio-One). Following overnight incubation at 37 °C/ 5% CO₂, plate wells were washed with Macrophage Infection Medium to remove non-adherent cells using ELx405 Select microplate washer (BioTek), and then filled with 40 μ L of Macrophage Infection Medium. *Leishmania donovani* HU3 splenic amastigotes isolated from infected spleens were re-suspended in Macrophage Infection Medium at a concentration of 6×10^7 cells/mL, and 10 μ L of the suspension were added to assay plate wells containing adherent macrophages. After a 24-hour infection period at 37 °C/ 5% CO₂, plate wells were washed with Macrophage Infection Medium to remove residual extracellular parasites and re-filled with 50 μ L of the medium. *Leishmania donovani*-infected macrophages were subsequently treated with DMSO-dissolved compounds (0.5% final DMSO concentration in the assay medium) in dose response for 120 hours at 37 °C/ 5% CO₂. Next, treated

macrophages were washed with the phosphate-buffered saline buffer (PBS; Sigma-Aldrich) supplemented with 0.5 mM magnesium chloride (Sigma-Aldrich) and 0.5 mM calcium chloride (Sigma-Aldrich), fixed with 0.4% paraformaldehyde (Sigma-Aldrich) in PBS, permeabilized with 0.1% Triton X-100 (Sigma-Aldrich) in PBS, and stained with SYBR Green I nucleic acid stain (Invitrogen, 1:100,000 dilution in PBS) overnight at 4 °C. Image collection and enumeration of macrophage cells and intracellular *L. donovani* amastigotes was performed using the OPERA QEHS automated confocal microscope system equipped with 20x water immersion objective (Evotec Technologies) and the OPERA Acapella software (Evotec Technologies) as described previously³².

All reported intra-macrophage *L. donovani* EC₅₀ values were calculated from at least 3 technical replicates (n= 3 or n= 4; specified in relevant Figure captions).

***Trypanosoma brucei* growth inhibition assay.** Bloodstream form *Trypanosoma brucei* List 427 parasites were continuously passaged in HMI-9 medium formulated from IMDM medium (Invitrogen), 10% heat-inactivated fetal bovine serum, 10% Serum Plus medium supplement (SAFC Biosciences), 1 mM hypoxanthine (Sigma-Aldrich), 50 µM bathocuproine disulfonic acid (Sigma-Aldrich), 1.5 mM cysteine (Sigma-Aldrich), 1 mM pyruvic acid (Sigma-Aldrich), 39 µg/mL thymidine (Sigma-Aldrich), and 14 µL/L beta-mercapthoethanol (Sigma-Aldrich); all concentrations of added components refer to those in complete HMI-9 medium. The parasites were cultured in 10 mL of HMI-9 medium in T75 CELL-STAR tissue culture flasks at 37 °C/ 5% CO₂.

To determine compound growth inhibitory potency on *T. brucei* bloodstream form parasites, 100 nL of serially diluted compounds in DMSO were transferred to the wells of white, solid bottom 384-well plates (Greiner Bio-One) by Echo 555 acoustic liquid handling system. Then, 5 x 10³ of *T. brucei* parasites in 40 µL of HMI-9 medium were added to each well, and the plates were incubated for 48 hours at 37 °C/ 5% CO₂. Parasite numbers in individual plate wells were determined through quantification of intracellular

ATP amount. The CellTiter-Glo luminescent cell viability reagent was added to plate wells, and ATP-dependent luminescence signal was measured on an EnVision MultiLabel Plate Reader. Luminescence values in wells with compounds were divided by the average luminescence value of the plate DMSO controls, and used for calculation of compound EC₅₀ values as described above.

Trypanosoma brucei EC₅₀ values shown in Fig. 1 and Extended Data Fig. 3 correspond to means of 4 technical replicates.

***Trypanosoma cruzi* amastigote growth inhibition assay.** NIH 3T3 fibroblast cells (ATCC) were maintained in RPMI 1640 medium (Life Technologies) supplemented with 10% heat-inactivated fetal bovine serum and 100 IU penicillin/ 100 µg/mL streptomycin at 37 °C/ 5% CO₂. *Trypanosoma cruzi* Tulahuen parasites constitutively expressing *Escherichia coli* beta-galactosidase³³ were maintained in tissue culture as an infection in NIH 3T3 fibroblast cells. Briefly, 2 x 10⁷ *T. cruzi* trypomastigotes were used to infect 6 x 10⁵ NIH 3T3 cells growing in T75 CELL-STAR tissue culture flasks and cultured at 37 °C/ 5% CO₂ until proliferating intracellular parasites lysed host 3T3 cells and were released into the culture medium (typically 6-7 days). During the infection, the tissue culture medium was changed every two days. Number of *T. cruzi* trypomastigotes present in one mL of medium was determined using a hemocytometer.

To determine compound potency on intracellular *T. cruzi* amastigotes, NIH 3T3 cells were re-suspended in phenol red-free RPMI 1640 medium containing 3% heat-inactivated fetal bovine serum and 100 IU penicillin/ 100 µg/mL streptomycin, seeded at 1,000 cells/ well (40 µL) in white, clear bottom 384-well plates (Greiner Bio-One), and incubated overnight at 37 °C/ 5% CO₂. The following day, 100 nL of each compound in DMSO were transferred to individual plate wells by Echo 555 acoustic liquid handling system. After one hour incubation, 1 x 10⁶ of tissue culture-derived *T. cruzi* trypomastigotes, in 10 µL of phenol red-free RPMI 1640 medium supplemented with 3% heat-inactivated fetal bovine serum and 100

474 IU penicillin/ 100 µg/mL streptomycin were added to each well. Plates were then incubated for 6 days at
475 37 °C/ 5% CO₂. Intracellular *T. cruzi* parasites were quantified by measuring the activity of parasite-
476 expressed beta-galactosidase. Ten microliters of a chromogenic beta-galactosidase substrate solution (0.6
477 mM chlorophenol red-β-D-galactopyranoside/ 0.6% NP-40 in PBS; both reagents from Calbiochem)
478 were added to each well and incubated for 2 hours at room temperature. After incubation, absorption was
479 measured at 570 nM on SpectraMax M2 plate reader (Molecular Devices). Measured absorbance values
480 in wells with compounds were divided by the average absorbance value of the plate DMSO controls, and
481 used for calculation of compound EC₅₀ values as described above.

482 *Trypanosoma cruzi* amastigote EC₅₀ values shown in Fig. 1 and Extended Data Fig. 3 correspond to
483 means of 4 technical replicates.

484 ***Trypanosoma cruzi* epimastigote proliferation assay.** *Trypanosoma cruzi* CL epimastigotes were
485 continuously passaged in LIT medium containing 9 g/L liver infusion broth (Difco), 5 g/L bacto-tryptose
486 (Difco), 1 g/L sodium chloride, 8 g/L dibasic sodium phosphate (Sigma-Aldrich), 0.4 g/L potassium
487 chloride (Sigma-Aldrich), 1 g/L D-glucose, 10 % heat-inactivated fetal bovine serum and 10 ng/mL of
488 hemin (Sigma-Aldrich). The medium was adjusted to pH= 7.2 with 6 M hydrochloric acid. The parasites
489 were cultured in 10 mL of LIT medium in T75 CELL-STAR tissue culture flasks at 27 °C.

490 To determine compound growth inhibitory potency on *T. cruzi* epimastigotes, 100 nL of serially diluted
491 compounds in DMSO were transferred to the wells of white, solid bottom 384-well plates (Greiner Bio-
492 One) by an Echo 555 acoustic liquid handling system. Then, 5 x 10³ of *T. cruzi* epimastigotes in 40 µL
493 of LIT medium were added to each well, and the plates were incubated for 7 days at 27 °C. Parasite
494 numbers in individual plate wells were determined through quantification of intracellular ATP amount.
495 The CellTiter-Glo luminescent cell viability reagent was added to plate wells, and ATP-dependent
496 luminescence signal was measured on an EnVision MultiLabel Plate Reader. Luminescence values in

497 wells with compounds were divided by the average luminescence value of the plate DMSO controls, and
498 used for calculation of compound EC₅₀ values as described above.

499 *Trypanosoma cruzi* epimastigote EC₅₀ values shown in Extended Data Fig. 4 correspond to means of 3
500 technical replicates.

501 **Mouse fibroblast NIH 3T3 growth inhibition assay.** NIH 3T3 fibroblast cells were maintained in
502 RPMI medium 1640 with glutamine (Life Technologies) supplemented with 5% heat-inactivated fetal
503 bovine serum and 100 IU penicillin/ 100 µg/mL streptomycin (3T3 Medium) at 37 °C/ 5% CO₂. NIH 3T3
504 fibroblast cells were purchased from ATCC. We did not perform cell line authentication and did not test
505 the cells for mycoplasma contamination. This cell line is not listed in the database of commonly
506 misidentified cell lines maintained by ICLAC and NCBI Biosample.

507 To determine compound potency, NIH 3T3 cells re-suspended in 3T3 medium were seeded at 1,000
508 cells/ well (50 µL) in white 384-well plates (Greiner Bio-One) and incubated overnight at 37 °C/ 5% CO₂.
509 The following day, 100 nL of each compound in DMSO were transferred to individual plate wells by
510 Echo 555 acoustic liquid handling system and plates were incubated for five days at 37 °C/ 5% CO₂. Cell
511 numbers in individual plate wells were determined through quantification of intracellular ATP amount.
512 The CellTiter-Glo luminescent cell viability reagent was added to plate wells, and ATP-dependent
513 luminescence signal was measured on an EnVision MultiLabel Plate Reader. Luminescence values in
514 wells with compounds were divided by the average luminescence value of the plate DMSO controls, and
515 used for calculation of compound CC₅₀ values as described above.

516 NIH 3T3 CC₅₀ values shown in Fig. 1 and Extended Data Fig. 3 correspond to means of 4 technical
517 replicates.

518 **Primary macrophage cytotoxicity assay.** Primary macrophage cell viability was determined on mouse
519 peritoneal macrophages infected with *L. donovani* and was expressed as the ratio of the number of

macrophage cells in wells treated with a compound to those in wells treated with DMSO. The number of macrophage cells in wells was determined by high content microscopy as described previously³². All reported macrophage CC₅₀ values were calculated from 4 technical replicates (n= 4; also specified in Figure 1 and Extended Data Figure 3 captions).

Selection of GNF3934- and GNF8000-resistant *T. cruzi* mutants. *T. cruzi* epimastigotes cultures resistant to GNF3943 and GNF8000 were generated using a methodology described previously³². Briefly, epimastigotes were initially cultured in the presence of compound concentration equivalent to its EC₂₀ value (GNF3943 EC₂₀= 1.5 μ M and GNF8000 EC₂₀= 0.2 μ M in 0.2% DMSO) or 0.2% DMSO (control). Once a week, parasites were counted and growth rates were determined. If the parasite cultures exhibited a reduced growth rate compared to 0.2% DMSO-treated parasites, epimastigotes were cultured at the same compound concentration. Once the growth rates matched that of the control epimastigote culture (0.2% DMSO), parasites were transferred into medium containing two-fold higher compound concentration. The process was repeated until significant resistance was achieved (~10- to 20-fold increase in corresponding EC₅₀ value). The time required for generation of cultures with such a level of resistance was approximately five months. Resistant clones were isolated via cloning by limiting dilution, and two independent clones were analyzed by whole genome sequencing.

***T. cruzi* whole genome sequencing.** Chromosomal DNA isolation from GNF3943- and GNF8000-resistant *T. cruzi* clones, whole genome sequencing and sequence analysis were performed as described previously³². Sequencing reads were aligned to the *T. cruzi* CL Brenner genome³⁴.

Generation of *T. cruzi* strains ectopically expressing proteasome beta 4 subunit variants. *PSMB4* TcCLB503891.100 was amplified from *T. cruzi* CL Brenner genomic DNA using KOD Hot Start DNA Polymerase (EMD Millipore), and sense (5'-AAAGCGGCCGCATGTCTGGAGACAACCATTG-3) and antisense (5'-CCATGATCTTGATGTAATATAAGGCATTCAGCCCTGCTG-3) primers. The

543 *PSMB4*^{F24L} gene was generated from the wild type *PSMB4* construct by site-directed mutagenesis using
 544 mutagenic sense (5-CAGCAGGGCTGAATGCCTTATATTACATCAAGATCATGG-3') and antisense
 545 (5'-CCATGATCTTGATGTAATATAAGGCATTCAGCCCTGCTG-3') primers and QuikChange II
 546 Site-Directed Mutagenesis Kit (Stratagene). The sequences of the wild type and mutant *PSMB4* genes
 547 were verified by sequencing and both gene versions were subcloned into the *T. cruzi* expression vector
 548 pTcIndex1 under control of a T7 promoter³⁵. *Trypanosoma cruzi* CL Brenner epimastigotes were first
 549 transfected as described previously³⁶ with the pLEW13 plasmid³⁷ harboring a tetracycline-inducible T7
 550 RNA polymerase gene. Transfected epimastigotes were selected in medium supplemented with neomycin
 551 (G418) at 500 µg/ml, and then transfected a second time with either pTcIndex1-*PSMB4*^{wt} or pTcIndex1-
 552 *PSMB4*^{F24L} plasmid. Double transfected epimastigotes were selected in the presence of 500 µg/mL of
 553 G418 (Sigma-Aldrich) and 500 µg/mL of hygromycin (Sigma-Aldrich). Susceptibility of double
 554 transfected epimastigote cell lines to compounds was assessed using induced (+5 mg/mL of tetracycline)
 555 and non-induced parasite cultures after five days of compound treatment. Parasite viability was
 556 determined with AlamarBlue (ThermoFisher Scientific).
 557 Reported EC₅₀ values for *T. cruzi* epimastigotes ectopically expressing PSMB4 proteins were calculated
 558 from 3 technical replicates (n= 3; also specified in the Figure 3a caption).
 559 **Generation of *T. brucei* strains ectopically expressing proteasome beta 4 subunit variants.** *PSMB4*
 560 (Tb927.10.4710) was amplified from *T. brucei* Lister 427 genomic DNA using PCR SuperMix High
 561 Fidelity (Invitrogen), sense (5'-GCAAGCTTATGGCAGAGACGACTATCGG-3) and antisense (5'-
 562 GCGGATCCCTAGCTTACAGATTGCACTC-3') primers. The *PSMB4*^{F24L} gene was generated from the
 563 wild type PSMB4 construct by site-directed mutagenesis using mutagenic sense (5'-
 564 gctgcgggggttaaatgcgttatactacattaagataacgg-3'), antisense (5'-ccgttatcttaatgtagtataacgcatttaaccccgagc-3')
 565 primers and QuikChange II Site-Directed Mutagenesis Kit (Stratagene). The sequences of the wild type

and mutant *PSMB4* genes were verified by sequencing and both gene versions were cloned into the *T. brucei* expression vector pHD1034 under control of a ribosomal RNA promoter. Transfected *T. brucei* Lister 427 cells were selected in medium supplemented with puromycin at 1 µg/ml. Susceptibility of transfected *T. brucei* cell lines to compounds were assessed after 2 days of compound treatment. Parasite viability was determined with CellTiter-Glo.

Reported EC₅₀ values for *T. brucei* parasites ectopically expressing PSMB4 proteins were calculated from 3 technical replicates (n= 3; also specified in the Figure 3b caption).

Purification of parasite 20S proteasomes. *T. cruzi* CL epimastigotes, *L. donovani* MHOM/SD/62/1S-CL2D axenic amastigotes and *T. brucei* Lister 27 bloodstream form trypomastigotes were grown to log phase and harvested by centrifugation. The corresponding cell pellets were stored at -80 °C until further use. Prior to purification, 10 g of cell pellets were thawed, re-suspended in lysis buffer (50 mM Tris-HCl pH = 7.5, 1 mM TCEP, 5 mM EDTA, and 10 µM E-64), and lysed by passing cell suspension three times through a needle (22 gauge) and by subsequent three freeze/ thaw cycles. The lysate was first cleared of cellular debris by two centrifugation steps (15,000 x g at 4 °C for 15 minutes followed by 40,000 x g at 4 °C for 60 minutes) and then fractionated through ammonium sulfate precipitation. The protein fraction precipitated between 45% and 65% of ammonium sulfate saturation was re-suspended in 25 mM Tris-HCl pH = 7.5, 1 mM TCEP buffer, and dialyzed overnight at 4 °C against the same buffer. Proteasomes were further purified by anion exchange chromatography (Resource Q column, GE Healthcare Life Sciences) and size exclusion chromatography (Superose 6 column, GE Healthcare Life Sciences) as described elsewhere³⁸. Active fractions from the latter purification step were pooled and used in proteasome biochemical assays.

Subunit composition analysis of purified *T. cruzi* 20S proteasome by LC/MS/MS. Purified *T. cruzi* proteasome sample was buffer-exchanged and concentrated into 100 mM trimethylamine bicarbonate-

HCl pH= 8.0, 150 mM NaCl buffer using a 10 kDa molecular weight cut-off micro-concentrator (Milipore Amicon Ultra). The resulting proteasome sample (200 µl, 1 mg/ml) was mixed with 5 µl of a TMTsixplex reagent (Pierce). After 60 second incubation to label primary amines, the reaction was stopped by adding 25 µl of 5% hydroxylamine. The labeled sample was run on 4-20% Bis-Tris PAGE gel (Invitrogen) to separate polypeptides. The gel was stained with eStain 2.0 (GenScript). Stained protein bands were cut out and in-gel digested separately with elastase (Promega) and asparaginase (Roche). Peptides generated by the digestions were resolved by HPLC using a vented column setup with a 2 cm Poros 10 R2 (Life Technologies, Carlsbad, CA) self-packed pre-column, and a PepMap Easy-Spray C18 analytical column (15 cm x 75 µm ID, Thermo Scientific). Resin-bound proteolytic fragments were eluted with 2 to 40% acetonitrile / 0.1% formic acid operated at 300 nL/min for 120 min. Spectra of eluted peptide species were determined by a column-coupled Q Exactive hybrid quadrupole orbitrap mass spectrometer (Thermo Scientific). Proteome Discoverer v1.4 software (Thermo Scientific) was used to search the *T.cruzi* genome²⁸ with identified spectra for presence of 20S proteasome subunits (Supplementary Table 7). Search parameters included fixed carbamidomethyl modification of cysteine, and variable oxidation of methionine, deamidation of asparagine, pyro-glu of N-terminal glutamine, and TMT(6-plex) modification of lysine residues.

Measuring proteasome proteolytic activities. The activity of purified parasite and human 20S proteasomes was monitored by measuring cleavage of various rhodamine-labelled fluorogenic substrates. Purified 20S proteasomes were diluted in proteasome assay buffer (25 mM Tris-HCl pH 7.5, 1 mM dithiothreitol (Sigma-Aldrich), 10 mM sodium chloride, 25 mM potassium chloride, 1 mM magnesium chloride, 0.05% (w/v) CHAPS (Sigma-Aldrich) and 0.9% DMSO) at a final concentration of 162 nM (parasite proteasomes) or 25 nM (human proteasome), and pre-incubated with compound (40 nL; 0.2% final DMSO concentration) for 1 hour. Next, the following substrates (Biosynthan GmbH) were added at

612 3 μ M final concentration to monitor specific proteolytic activities (Suc-LLVY-Rh110-dPro:
 613 chymotrypsin-like activity; Ac-RLR-Rh110-dPro: trypsin-like activity; Ac-GPLD-Rh110-dPro: caspase-
 614 like activity). The reaction was allowed to proceed for two hours at room temperature and fluorescence as
 615 a measure of purified 20S proteasome activity was monitored using the EnVision® plate reader
 616 (excitation at 485 nm/ emission at 535 nm). Km and Ki values were calculated using GraphPad Prism
 617 (GraphPad Software) 'Non-competitive enzyme inhibition' function.

618 Data shown in Fig. 4a, 4c, 4d and Extended Data Table 3 represent means of 3 technical replicates (n= 3).
 619 Data shown in Fig. 4b and Extended Data Fig. 5 represent means of 2 technical replicates (n= 2).

620 **Monitoring accumulation of ubiquitylated proteins in intact cells.** Growing *T. cruzi* epimastigotes
 621 were seeded into 24-well tissue culture plate (1×10^7 cells/per well) in LIT medium and treated for 2-12
 622 hours with DMSO (0.2%) or various concentrations of bortezomib and GNF6702 at 27 °C. Following the
 623 treatment, parasites were collected by centrifugation (3,500 g for 6 minutes) and washed twice with
 624 phosphate-buffered saline (PBS). Epimastigotes were lysed by resuspending washed cells in a buffer
 625 containing 50 mM Tris-HCl pH= 7.4, 150 mM sodium chloride, 1% CHAPS, 20 μ M E-64 (Sigma-
 626 Aldrich), 10 mM EDTA(Sigma-Aldrich), 5 mM N-ethylmaleimide(Sigma-Aldrich), 1 mM
 627 phenylmethylsulfonyl fluoride (Sigma-Aldrich), 10 μ g/mL leupeptin (Sigma-Aldrich), 10 μ g/mL
 628 aprotinin (Sigma-Aldrich), and incubating the suspension on ice for 20 minutes. Cell lysates were cleared
 629 by centrifugation at 21,000 g for 30 min at 4 °C.

630 For 3T3 cells, 2×10^5 cells/ well were seeded into 24-well tissue culture plates in RPMI medium 1640
 631 supplemented with 10% heat-inactivated fetal bovine serum, and incubated overnight at 37 °C to allow
 632 cells to attach. Attached cells were treated for 2 hours with DMSO (0.25%) or various concentrations of
 633 bortezomib and GNF6702. Treated cells were washed twice with PBS and then lysed by incubating cells
 634 in modified RIPA buffer (50 mM Tris-HCl pH= 7.4, 1% Triton X-100, 0.2% sodium dodecylsulfate, 1

mM EDTA, 1 mM phenylmethylsulfonyl fluoride, 5 µg/mL aprotinin, 5 µg/mL leupeptin) for 30 min at 4 °C. Cell lysates were cleared by centrifugation at 21,000 g for 30 min at 4 °C.

Protein concentration in cell extracts was determined with BCA assay (ThermoFisher), and 10 µg of cell extracts were loaded on NuPAGE Novex 4-12% Bis-Tris gel (Invitrogen). After electrophoresis, resolved proteins were transferred to nitrocellulose membrane. Ubiquitylated proteins were detected with polyclonal anti-ubiquitin primary antibody (Proteintech, catalogue number 10201-2-AP) and rabbit anti-mouse IgG-peroxidase antibody (Sigma-Aldrich, catalogue number A0545), and then imaged using ECL Prime Western Blotting Detection Reagent (Amersham) on Chemidoc XR+ imaging system (BioRad). Collected western blot images were quantified using Image Lab software (BioRad). Briefly, rectangles of identical size and shape were drawn around each blot lane to include inside the shape all ubiquitylated protein bands within 17 - 198 kDa molecular mass range. Next, integrated signal intensities within the rectangles (reported by the Image Lab software) were used for calculation of EC₅₀ values. Three technical replicate experiments (n= 3) for each different dose response experiment (GNF6702 on *T. cruzi* epimastigotes; GNF6702 on 3T3 cells; bortezomib on *T. cruzi* epimastigotes; bortezomib on 3T3 cells) were performed.

***Trypanosoma cruzi* proteasome modeling studies.** The homology model of *T. cruzi* 20S proteasome was built using ‘Prime’ protein structure prediction program (Schrödinger) and X-ray structure of bovine 20S proteasome (pdb accession code 1IRU)³⁹ as the template. The model was subjected to restrained minimization to relieve inter-chain clashes. ‘SiteMap’ program (Schrödinger) was used to identify pockets on a protein surface suitable for small molecule binding. Flexible ligand docking was performed using ‘Glide 5.8’ (Schrödinger). The grid box was centered in a middle of the identified pocket and extended by 10 Å, with outer box extending additional 20Å. The ligand was docked using the standard

657 precision (SP) algorithm and scored using 'GlideScore' (Schrödinger). The GNF6702 GlideScore is
658 equal to -8.5.

659 **Receptor, enzyme and ion channel assays.** GNF6702 profiling was performed at 10 μ M concentration
660 in a selectivity panel at Eurofins (www.eurofinspanlabs.com/Catalog/AssayCatalog/AssayCatalog.aspx).
661 Listed values % change in the assay readout relative to the DMSO control. To determine inhibition of a
662 subset of human tyrosine kinases by GNF6702, the inhibitor was profiled on a panel of Ba/F3 cell lines
663 expressing individual Tel-activated kinases as described previously⁴⁰. All assays were performed as
664 single technical repeats.

665 **Determination of GNF6702 thermodynamic solubility.** The solubility of GNF6702 was assessed in a
666 high throughput thermodynamic solubility assay as described previously⁴¹. First, 25 μ L of GNF6702
667 DMSO solutions were transferred to individual wells of a 96-well plate. DMSO was evaporated and 250
668 μ L of 67 mM potassium phosphate buffer pH 6.8 were added to yield projected final compound
669 concentrations from 1 μ M to 100 μ M. The plate was sealed to prevent solvent loss and shaken for 24
670 hours at room temperature. The plate was then filtered to remove non-dissolved material. Concentration
671 of GNF6702 in individual plate wells was determined by measuring solution UV absorbance with
672 reference to a GNF6702 calibration curve.

673 **Determination of GNF6702 permeability in Caco-2 assay.** A 96-Multiwell Insert System (BD
674 Biosciences) was used for the Caco-2 cell culture and permeability assay as described previously⁴². Caco-
675 2 cells were seeded onto insert wells at a density of 1.48×10^5 cells per ml and allowed to grow for 19-23
676 days before assays. To measure both absorptive (apical to basolateral [A-B]) and secretory (basolateral to
677 apical [B-A]) compound transport, a solution of GNF6702 at 10 μ M concentration in 0.5% DMSO were
678 added to donor wells. The plate was incubated at 37°C for 2 hours, with samples taken at the beginning

679 and end of the incubation from both donor and acceptor wells. The concentration of GNF6702 was
680 determined by LC-MS/MS.

681 Apparent drug permeability (P_{app}) was calculated using the following equation:

682
$$P_{app} = dQ/dt * 1/(A * C_{in})$$

683 where dQ/dt is the total amount of a test compound transported to the acceptor chamber per unit of time
684 (nmol/s), A is the surface area of the transport membrane (0.0804 cm^2), C_{in} is the initial compound
685 concentration in the donor chamber ($10 \text{ }\mu\text{M}$), and P_{app} is expressed as cm/s).

686 **Determination of human CYP450 inhibition by GNF6702.** Extent of inhibition of major human
687 CYP450 isoforms 2C9, 2D6 and 3A4 by GNF6702 was determined using pooled human liver
688 microsomes and the known specific substrates of various CYP450 isoforms: diclofenac ($5 \text{ }\mu\text{M}$), bufuralol
689 ($5 \text{ }\mu\text{M}$), midazolam ($5 \text{ }\mu\text{M}$), and testosterone ($50 \text{ }\mu\text{M}$). Probe substrate concentrations were used at
690 concentrations equal to their reported K_m values. The CYP450 inhibition assays with probe substrates
691 diclofenac (2C9) or midazolam (3A4) were incubated at $37 \text{ }^\circ\text{C}$ for 5 to 10 minutes using a microsomal
692 protein concentration of 0.05 mg/mL . Probe substrates bufuralol (2D6) and testosterone (3A4) were
693 incubated at $37 \text{ }^\circ\text{C}$ for 20 minutes using microsomal concentration 0.5 mg/mL . The test concentrations of
694 GNF6702 ranged from 0.5 to $25 \text{ }\mu\text{M}$ in the presence of 1% DMSO. The reactions were initiated by
695 adding NADPH (1 mM final concentration; Sigma-Aldrich) after a 5-min pre-incubation. Incubations
696 were terminated by the addition of $300 \text{ }\mu\text{L}$ of acetonitrile to $100 \text{ }\mu\text{L}$ of a sample. No significant
697 cytochrome P450 inhibition was observed. Extent of CYP450 isoform inhibition was determined by
698 quantifying residual concentrations of individual CYP450 substrate probes at the end of reactions by
699 LC/MS/MS.

700 **Determination of GNF6702 *in vitro* metabolic stability.** The intrinsic metabolic stability of GNF6702
701 was determined in mouse and human liver microsomes using the compound depletion approach and

LC/MS/MS quantification. The assay measured the rate and extent of metabolism of GNF6702 by measuring the disappearance of the compound. The assay determined GNF6702 *in vitro* half-life ($T^{1/2}$) and hepatic extraction ratios (ER) as described previously⁴³. GNF6702 was incubated for 30 minutes at 1.0 μ M concentration in a buffer containing 1.0 mg/ mL liver microsomes. Samples (50 μ L) were collected at 0, 5, 15 and 30 minutes and immediately quenched by addition of 150 μ L of ice-cold acetonitrile/ methanol/water mixture (8/1/1). Quantification of GNF6702 in samples was performed by LC/MS/MS, and the *in vitro* intrinsic clearance was determined using the substrate depletion method. The intrinsic clearance, CL_{int} was calculated using the following equation:

$$CL_{int} = (0.693/ T^{1/2}) * (V/ M) ,$$

where $T^{1/2}$ is the *in vitro* half-life, V (μ L) is the reaction volume, and M (mg) is the microsomal protein amount. Finally the hepatic extraction ratio is calculated as:

$$ER = CL_h/Q_h ,$$

where CL_h = hepatic clearance, Q_h = hepatic blood flow.

CL_h was calculated using the following equation:

$$CL_h = (Q_h * f_u * CL_{int}) / (Q_h + f_u * CL_{int}) ,$$

where f_u = fraction unbound to protein (assumed to be 1).

Pharmacokinetic studies. An outline of various *in vitro* and *in vivo* DMPK assays used in this study for compound profiling was summarized previously⁴⁴. The pharmacokinetic properties of GNF compounds and calculation of pharmacokinetic parameters was performed as described previously²³. Mean compound plasma concentrations were calculated from fitted functions approximating compound plasma profile throughout 8 days of dosing. Blinding was not possible in these experiments.

Bioanalysis of GNF6702 in plasma. Plasma concentration of GNF6702 was quantified using a LC/MS/MS assay. Solution of 20 ng/mL of verapamil hydrochloride (Sigma-Aldrich) in

725 acetonitrile/methanol mixture (3/1 by volume), was used as an internal standard. Twenty microliters of
726 plasma samples were mixed with 200 μ l of internal standard solution. The samples were vortexed and
727 then centrifuged in an Eppendorf Centrifuge 5810R (Eppendorf) at 4,000 rpm for 5 minutes at 4 °C to
728 remove precipitated plasma proteins. The supernatants (150 μ l) were transferred to a 96-well plate and
729 mixed with 150 μ l H₂O. The samples (10 μ l) were then injected onto a Zorbax SB-C8 analytical column
730 (2.1 x 30 mm, 3.5 μ m; Agilent Technologies) and separated using a three step gradient (1st step: 1.5 mL
731 of 0.05% formic acid in 10% acetonitrile; 2nd step: 0.5 mL of 0.05% formic acid in 100% acetonitrile; 3rd
732 step: 0.5 mL of 0.05% formic acid in 10% acetonitrile) at flow rate of 700 μ l/min. GNF6702 and
733 verapamil were eluted at retention time 1.19 and 1.17 minutes, respectively. The HPLC system,
734 consisting of Agilent 1260 series binary pump (Agilent Technologies), Agilent 1260 series micro
735 vacuum degasser (Agilent Technologies) and CTC PAL-HTC-xt analytics autosampler (LEAP
736 Technologies) was interfaced to a SCIEX API 4000 triple quadrupole mass spectrometer (Sciex). Mass
737 spectrometry analysis was carried out using atmospheric pressure chemical ionization (APCI) in the
738 positive ion mode. GNF6702 (430.07 > 333.20) and verapamil (455.16 > 164.90) peak integrations were
739 performed using AnalystTM 1.5 software (Sciex). The lower limit of quantification (LLOQ) in plasma
740 was 1.0 ng/mL. Samples were quantified using seven calibration standards (dynamic range 1 – 5,000
741 ng/mL) prepared in plasma and processed as described above.

742 **Formulation of study drugs for *in vivo* efficacy experiments.** All compounds administered to mice
743 during efficacy experiments were formulated as suspensions in distilled water containing 0.5%
744 methylcellulose (Sigma-Aldrich) and 0.5% Tween 80 (Sigma-Aldrich). During a treatment course, each
745 mouse received 0.2 ml of drug suspension per dose by oral gavage.

746 **Mouse model of visceral leishmaniasis.** Female BALB/c mice (Envigo; 6-8 weeks old) were infected by
747 tail vein injection with 4×10^7 *L. donovani* MHOM/ET/67/HU3 splenic amastigotes (protocol number

P11-319). Seven days after infection, animals were orally dosed for eight days with vehicle (0.5% methylcellulose/ 0.5% Tween 80, miltefosine (12 mg/kg once-daily; Sigma-Aldrich), or a GNF compound (twice-daily). On the first day of dosing, three mice were used for collection of blood for PK determination and euthanized afterwards. On the last day of dosing, PK samples were collected from remaining five mice, which were also used for determination of compound efficacy (n= 5 mice per group). Liver samples were collected from these five mice and *L. donovani* parasite burdens were quantified by qPCR as follows. Total DNA was extracted from drug-treated mice livers using the DNeasy Blood and Tissue Kit (Qiagen). Two types of DNA were quantified in parallel using the TaqMan assay: *L. donovani* major surface glycoprotein gp63 (Ldon_GP63) and mouse GAPDH. *L. donovani* GP63 DNA was quantified with the following set of primers: TGCGGTTTATCCTCTAGCGATAT (forward), AGTCCATGAAGGCGGAGATG (reverse), and TGGCAGTACTTCACGGAC (TaqMan MGB probe, 5'-FAM-labeled reporter dye, non-fluorescent quencher). Mouse GAPDH DNA was quantified with the following set of primers: GCCGCCATGTTGCAAAC (forward primer), CGAGAGGAATGAGGTAGTCACAA (reverse primer), and ATGAATGAACCGCCGTTAT (TaqMan MGB probe, 5'-FAM-labeled reporter dye, non-fluorescent quencher). Each qPCR reaction (10 µL) included 5 µl of TaqMan Gene Expression Master Mix (Life Technologies), 0.5 µL of a 20X primer/probe mix (Life Technologies), and 4.5 µL (50 ng) of total DNA from liver samples. DNA amount was quantified using the Applied Biosystems 7900HT instrument. *L. donovani* parasite burden (RU: relative units) was expressed as the abundance of *L. donovani* GP63 DNA relative to the abundance of mouse GAPDH DNA.

Mouse footpad model of cutaneous leishmaniasis. *L. major* MHOM/SA/85/JISH118 metacyclic promastigotes were generated and purified by the peanut agglutinin method as described elsewhere⁴⁵. To establish the *L. major* footpad infection, female BALB/c mice (Envigo; 6-8 weeks old; protocol number

P11-319) were injected with suspension of *L. major* metacyclic promastigotes (1×10^6 parasites in 50 μ L) into each hind footpad. After eight days of infection, animals were dosed with vehicle, miltefosine (30 mg/kg once-daily), or indicated regimens of GNF6702 for seven days (n=6 mice per group). The progress of infection was monitored by measuring the size (length and thickness) of hind footpad swelling using digital calipers. At the end of the study, the mice were euthanized, and the footpad tissues were extracted and used for genomic DNA isolation with the DNeasy Blood and Tissue kit (Qiagen). The *L. major* footpad burden was determined by qPCR quantification of kinetoplastid minicircle DNA (forward primer: 5'-TTTTACACCTCCCCCAGTTT-3'; reverse primer: 5'-CCCGTTCATAATTTCCCGAAA-3'; Taqman MGB probe: 5'-AGGCCAAAAATGG-3', 5'-FAM [6-carboxyfluorescein]-labeled reporter dye, non-fluorescent quencher). The amounts of mouse chromosomal DNA in extracted samples were quantified in parallel qPCR using a glyceraldehyde-3-phosphate dehydrogenase (GAPDH) TaqMan assay as described for mouse VL model above. *L. major* burden in footpad was expressed as the ratio of kinetoplast minicircle DNA to mouse GAPDH. P values for the between-groups differences in efficacies were calculated with a Student's paired t test with a two-tailed distribution.

Mouse model of Chagas disease. Compound efficacy in mouse model of Chagas disease was determined as described previously²³. Female C57BL/6 mice (Envigo; 6-8 weeks old; protocol number P11-316) were infected by intraperitoneal injection with 10^3 tissue culture-derived *T. cruzi* CL trypomastigotes. Starting at 35 days after infection, the animals were dosed orally once-daily with 100 mg/kg benznidazole (Sigma-Aldrich) and indicated doses of GNF6702 (1, 3, and 10 mg/kg twice-daily, n=8 per group) for 20 days. Ten days following the end of drug treatment, the mice underwent four cycles of cyclophosphamide immunosuppression, each cycle lasting one week. During each immunosuppression cycle, mice were dosed by oral gavage once-daily with 200 mg/kg

cyclophosphamide (suspension in 0.5% methylcellulose/ 0.5% Tween80 aqueous solution) on day 1 and day 4 of the cycle. After the fourth immunosuppression cycle, blood samples were collected from the orbital venous sinus of each mouse, mice were euthanized and heart and colon samples were collected. Samples from treated mice were used for extraction of total DNA using the High Pure PCR template preparation kit (Roche). The amounts of *T. cruzi* satellite DNA (195-bp fragment) in extracted DNA samples were quantified by real-time qPCR TaqMan assay (Life Technologies) with the following set of primers: AATTATGAATGGCGGGAGTCA (forward primer), CCAGTGTGTGAACACGCAAAC (reverse primer), and AGACACTCTCTTTCAATGTA (TaqMan MGB probe, 5'-FAM [6-carboxyfluorescein]-labeled reporter dye, non-fluorescent quencher). The amounts of mouse chromosomal DNA in extracted samples were quantified in parallel qPCR reactions using a GAPDH (glyceraldehyde-3-phosphate dehydrogenase) TaqMan assay as described for mouse VL model above. Each qPCR mixture (10 µl) included 5 µl of TaqMan Gene Expression master mix (Life Technologies), 0.5 µl of a 20x primer/ probe mix (Life Technologies), and 4.5 µl (50 ng) of total DNA extracted from blood samples. PCRs were run on the Applied Biosystems 7900HT instrument. *T. cruzi* parasitemia was expressed as the abundance of *T. cruzi* microsatellite DNA relative to the abundance of mouse GAPDH DNA.

Mouse model of stage II HAT. Female CD1 (Charles River UK; ~8 weeks old; protocol number PPL 60/4442) mice were infected by injection into the peritoneum with 3×10^4 *T. brucei* (GVR35-VSL2) bloodstream form parasites⁴⁶. Starting on day 21, mice were dosed by oral gavage once-daily with GNF6702 (n= 6) at 100 mg/kg for 7 days or a single dose of diminazene aceturate (Sigma-Aldrich) at 40 mg/kg in sterile water was administered by ip injection (n= 3). A group of untreated mice (n= 3) was included as controls.

Mice were monitored weekly for parasitemia from day 21 post-infection. *T. brucei* was quantified in blood samples from the tail vein by microscopy, and *in vivo* bioluminescence imaging of infected mice was performed before treatment on day 21 post-infection and in weeks following the treatment (day 28, 35, 42, 56, 63, 72, 84, 92 post-infection). Imaging on groups of three mice was performed 10 min after ip injection of 150 mg D-luciferin (Promega)/kg body weight (in PBS) using an IVIS Spectrum (PerkinElmer) as described previously²⁵. A group of uninfected mice (aged-matched for day 0 time point; n= 4) were imaged using the same acquisition settings to show the background bioluminescence (Fig. 2e, grey-filled squares) in the absence of luciferase-expressing *T. brucei* after day 92 of the experiment. Untreated and diminazene-treated mice were euthanized on days 32 and 35, and day 42, respectively, due to high parasitemia or the development of symptoms related to CNS infection. GNF6702-treated mice were euthanized on day 92. No parasitemia or clinical symptoms were observed at this point. At the specified endpoints mice were sacrificed by cervical dislocation, after which whole brains were removed and imaged *ex vivo* within 10 minutes after administration of 100 μ L of D-luciferin onto the brain surface. Data analysis for bioluminescence imaging was performed using Living Image Software. The same rectangular region of interest (ROI) covering the mouse body was used for each whole body image to show the bioluminescence in total flux (photons per second) within that region. Image panels of whole mouse bodies are composites of the original images with areas outside the ROI cropped out to save space. For *ex vivo* brain images the same oval shaped ROI was used to display the bioluminescence detected for each mouse brain at the respective endpoints.

Chemical synthesis. The detailed procedures for chemical synthesis are presented in Supplementary Information.

END NOTES

Supplementary Information can be found at the end of this manuscript.

Acknowledgements This work was supported in part by grants from the Wellcome Trust (091038/Z/09/Z to R.J.G. and F.S., and 104976/Z/14/Z, 104111/15/Z to J.C.M. and E.M.) and NIH (AI106850 to F.S.B.). We thank Simon Croft, Rob Don, Lars Gredsted, Alan Hudson and John Mendlein for discussions, Rick Tarleton for *T. cruzi* CL strain, and George Cross for *T.b. brucei* Lister 427 strain. We thank Andreas Kreusch for help with proteasome purification, and Fabio Luna for help with *T. cruzi* whole genome sequencing. We acknowledge technical assistance of Omeed Faghieh in generating the plasmids for ectopic expression of *PSMB4* in *T. cruzi*, Ryan Ritchie for IVIS *in vivo* imaging, and Annie Mak, Jason Matzen and Paul Anderson for execution of high throughput screens. We thank John Isbell and Thomas Hollenbeck for profiling GNF6702 in ADME assays.

Contributions

A.B., F.L., C.J.N.M., P.K.M., A.S.N., J.L.T. and V.Y. designed chemical analogues, and performed chemical synthesis and purification of synthesized analogues. F.S.B., J.B., J.R.G., S.K., H.X.Y.K., Y.H.L., S.P.S.R., F.S., and X.L. conducted and analyzed data from *in vitro* growth inhibition assays. L.C.D., X.L., J.C.M., E.M., I.C.R., S.P.S.R., M.S., F.S., and B.G.W. conducted and analyzed data from *in vivo* efficacy assays. J.B., M.-Y.G., S.K., and F.S. conducted proteasome purification, proteasome inhibition assays and biochemical data analysis. S.W.B., G.F., S.K., F.S., and J.R.W. designed, conducted and analyzed experiments resulting in identification of proteasome resistance mutations. G.S. and B.B. built the homology model of *T. cruzi* proteasome structure and performed GNF6702 docking. A.B. and J.D.V. analyzed *T. cruzi* proteasome by mass spectrometry. A.N., T.G., M.S., F.S., and T.T. designed, conducted, and analyzed PK data. A.N. and V.M. led the chemistry team. F.S. led the biology team. R.J.G. and F.S. supervised and led the overall project, and led the writing of the manuscript. All authors contributed to writing of the manuscript.

Author affiliations

¹Genomics Institute of the Novartis Research Foundation, San Diego, California 92121, USA. ²Wellcome Trust Centre for Molecular Parasitology, Institute of Infection, Immunity and Inflammation, College of Medical, Veterinary and Life Sciences, University of Glasgow, Glasgow G12 8TA, UK. ³Centre for Immunology and Infection, Department of Biology, University of York, Wentworth Way, Heslington, York, YO10 5DD, UK. ⁴Department of Medicine, University of Washington, Seattle, Washington 98109, USA. ⁵Novartis Institute for Tropical Diseases, Singapore.

Author information

*These authors contributed equally to this work.

Competing financial interests

Patents related to this work has been filed (WO 2015/095477 A1, WO 2014/151784 A1, WO 2014/151729). Several authors own shares of Novartis.

Corresponding authors

Correspondence and requests for materials should be addressed to F. S. (fsupek@gnf.org)

EXTENDED DATA LEGENDS

Extended Data Figure 1: Pharmacokinetic profile of GNF6702 in mouse. a, Time profiles of mean free plasma concentration of GNF6702 in mouse model of visceral leishmaniasis; free GNF6702 concentration values were predicted from measured total plasma concentration values collected on day 1 and day 8 of treatment. Dashed blue lines correspond to intra-macrophage *L. donovani* EC₅₀ of 18 ± 1.8 nM and EC₉₉ of 42 ± 5.6 nM. Circles: means ± s.d.; n=3 mice for treatment day 1; n=5 mice for treatment day 8; fraction unbound in mouse plasma=0.063. For data points lacking error bars, standard deviations are smaller than circles representing means. **b,** Time course of total GNF6702 concentration in mouse plasma and brain after single oral dose (20 mg/kg); n=2 mice per time point; circles: measured values; rectangles: means.

Extended Data Figure 2: GNF6702 clears parasites from mice infected with *T. brucei*. **a,** *In vivo*
 quantification of bioluminescent *T. brucei* in infected mice before and after treatment. ip: intraperitoneal;
 day 21: start of treatment; day 28: 24 hours after last GNF6702 dose; day 42: evaluation of early parasite
 recrudescence in mice treated with diminazene aceturate (n=3); day 42 and 92: absence of parasite
 recrudescence in mice treated with GNF6702 (n=6). Images from uninfected mice (3 mice of 4 are shown)
 aged-matched for day 0 were collected independently using the same acquisition settings. Parasitemia
 (blue font) and whole mouse total flux (black font) values of each animal are shown above the image;
 N.D.: not detectable. Within each group the mouse numbers in yellow (top left in each image) refer to the
 same mouse imaged throughout. Complete sets of parasitemia and whole mouse total flux values
 collected on individual mice throughout the experiment are listed in Supplementary Tables 4 and 5. **b,**
 Brains from mice shown in panel a were soaked in luciferin and imaged for presence of bioluminescent *T.*
brucei at the indicated time points. For three diminazene-treated mice, two images of each brain are
 shown, one at a lower sensitivity (left) and the other at a high signal intensity scale.

**Extended Data Figure 3: Structures and profiles of GNF3943 and GNF8000 used for selection of
 resistant *T. cruzi* lines.** *L. donovani*: amastigotes proliferating within primary mouse macrophages; *T.*
brucei: the bloodstream form trypomastigotes; *T. cruzi*: amastigotes proliferating in 3T3 fibroblast cells;
 macrophage: mouse primary peritoneal macrophages; EC₅₀ and CC₅₀: half-maximum growth inhibition
 concentration; F: oral bioavailability in mouse after administering single compound dose (20 mg/kg) as a
 suspension; CL: plasma clearance in mouse after single iv bolus dose (5 mg/kg); all EC₅₀ and CC₅₀
 values correspond to means \pm s.e.m. (n=4 technical replicates).

**Extended Data Figure 4: Mutations in proteasome beta 4 subunit confer resistance to GNF6702 in
T. cruzi and *T. brucei*.** **a,** growth curves of wild type, GNF3943-resistant and GNF8000-resistant *T.*
cruzi epimastigote strains in the presence of increasing concentrations of GNF6702, nifurtimox,

bortezomib and MG132; RU (relative units) corresponds to parasite growth relative to the DMSO control (%); for data points lacking error bars, standard errors are smaller than circles representing means; due to limited aqueous solubility, the highest tested GNF6702 concentration was 10 μ M. **b**, growth inhibition EC₅₀ values of GNF6702, bortezomib, MG132 and nifurtimox on indicated *T. cruzi* strains. **c**, growth inhibition EC₅₀ values of GNF6702 and bortezomib on *T. cruzi* epimastigotes and *T. brucei* bloodstream form trypomastigotes overexpressing PSMB4^{WT} or PSMB4^{F24L}. Data shown in panels **a**, **b** and **c** correspond to means \pm s.e.m. (n=3 technical replicates).

Extended Data Figure 5: Correlation between inhibition of parasite proteasome chymotrypsin-like activity and parasite growth inhibition by the GNF6702 compound series. IC₅₀: half-maximum inhibition of indicated parasite proteasome; *T. brucei* EC₅₀: half-maximum growth inhibition on *T. brucei* bloodstream form trypomastigotes; *T. cruzi* EC₅₀: half-maximum growth inhibition on *T. cruzi* amastigotes proliferating inside 3T3 cells; data points correspond to means of 2 technical replicates; red circles: IC₅₀>20 μ M; yellow circles: IC₅₀>20 μ M and EC₅₀>25 μ M; data for 317 analogues are shown.

Extended Data Figure 6: Hypothetical model of GNF6702 binding to *T. cruzi* proteasome beta 4 subunit. **a**, Alignment of amino acid sequences of proteasome beta 4 subunits (PSMB4) from *L. donovani*, *T. cruzi*, *T. brucei* and *H. sapiens*. Green: amino acid residues conserved between human and kinetoplastid PSMB4 proteins; blue: amino acid residues conserved only among kinetoplastid PSMB4 proteins; black: amino acids mutated in *T. cruzi* mutants resistant to analogues from the GNF6702 series. **b**, Surface representation of the modeled *T. cruzi* 20S proteasome structure showing relative positions of the beta 5 and beta 4 subunits. Beta 4 amino acid residues F24 and I29 (colored yellow) are located at the interface of the two beta subunits. GNF6702 is depicted in a sphere representation bound into a predicted pocket on the beta 4 subunit surface with carbon, nitrogen, oxygen and hydrogen atoms colored magenta, blue, red and grey, respectively. The other *T. cruzi* 20S proteasome subunits are colored gray. **c**, Close-up

of the beta 5 and beta 4 subunits. The beta 5 subunit active site (pocket 1, chymotrypsin-like activity) is colored pale green. The predicted beta 4 pocket (pocket 2) with bound GNF6702 is colored blue. The inhibitor is shown in a stick representation with atoms colored as described in caption for the b panel. Beta 4 residues F24 and I29 are colored yellow. The proteasome model shown in panels b and c was produced by The PyMol Molecule Graphics System, Version 1.8, Schrodinger, LLC.

Extended Data Figure 7: Effect of GNF6702 on accumulation of ubiquitylated proteins by *T. cruzi* epimastigotes and 3T3 cells. **a**, Western blot analysis of *T. cruzi* whole cell extracts with anti-ubiquitin antibody after treatment with GNF6702 and bortezomib. **b**, Western blot analysis of 3T3 whole cell extracts with anti-ubiquitin antibody after treatment with GNF6702 and bortezomib. **c**, Concentrations of GNF6702 and bortezomib effecting half-maximum accumulation of ubiquitylated proteins in *T. cruzi* and 3T3 cells (means \pm s.e.m.; n=3 technical replicates); total ubiquitin signal values in individual blot lanes shown in panels **a** and **b** were quantified and used for calculation of the listed EC₅₀ values. In **a** and **b**, numbers above the blot lanes indicate compound concentrations and D indicates control, DMSO-treated cells. For western blot source data, see Supplementary Figure 1.

Extended Data Table 1: Point mutations identified by whole genome sequencing in GNF3943- and GNF8000-resistant *T. cruzi* epimastigotes.

Extended Data Table 2: Enzyme inhibition IC₅₀ values of bortezomib and GNF6702 on three proteolytic activities of wild type *T. cruzi*, PSMB4^{I29M} *T. cruzi*, and *H. sapiens* proteasomes.

Extended Data Table 3: Inhibition kinetics parameters of GNF6702 on *L. donovani* and *T. cruzi* proteasomes.

SUPPLEMENTARY METHODS

1. Genomics Institute of the Novartis Research Foundation (GNF) chemical library

The GNF chemical library consists of ~3 million low molecular weight compounds.

955 **2. High throughput screening (HTS) campaigns and hit identification**

956 The high throughput screens were performed using 1,536 well polystyrene solid bottom white
957 microplates (Greiner Bio-One). The GNF chemical library was tested against *L. donovani*, *T. brucei* and
958 *T. cruzi* in whole-cell growth inhibition screens at single compound concentrations specified in sections
959 below describing individual parasite screens. Parasite proliferation protocols described in the Methods
960 section were optimized for 1,536 well plate assay format to provide optimal assay window and Z-factor.
961 Primary hits included compounds that reduced growth of parasites by more than 50% relative to the
962 relevant DMSO controls.

963 **2.1. *Leishmania donovani* HTS**

964 *Leishmania donovani* MHOM/SD/62/1S-CL2D axenic amastigotes in cell suspension were dispensed
965 into 1,536-well assay plates (2,000 parasite cells in 5 μ L of medium) and library compounds dissolved in
966 DMSO were added to 4 μ M final concentration (0.4% final DMSO concentration). After 48 hour
967 incubation at 37 °C, parasite viability was assessed using the CellTiter-Glo Luminescent Cell Viability
968 Assay (Promega) as described previously³². Compounds causing more than 50% reduction in parasite
969 viability were considered hits. Identified hits were subsequently evaluated in the screening assay in
970 triplicates at 4 μ M compound concentration. Compounds that inhibited *L. donovani* growth in at least
971 two replicates were considered confirmed hits.

972 **2.2. *Trypanosoma brucei* HTS**

973 *Trypanosoma brucei* Lister 427 bloodstream trypomastigotes in cell suspension were dispensed into
974 1,536-well assay plates (900 parasite cells in 7 μ L of medium) and library compounds dissolved in
975 DMSO were added to 7 μ M final concentration (0.7% final DMSO concentration). After 48 hour
976 incubation at 37 °C, parasite viability was assessed using the CellTiter-Glo Luminescent Cell Viability
977 Assay (Promega) as described previously³². Compounds causing more than 50% reduction in parasite

viability were considered hits. Identified hits were subsequently evaluated in the screening assay in triplicates at 7 μ M compound concentration. Compounds that inhibited *T. brucei* growth in at least two replicates were considered confirmed hits.

2.3. *Trypanosoma cruzi* HTS

A suspension of mouse fibroblast 3T3 cells was dispensed into 1,536-well assay plates (750 cells in 5 μ L of medium). After overnight incubation at 37 °C, adhered 3T3 cells were infected with *T. cruzi* trypomastigotes (2,500 trypomastigotes per well in 3 μ L of medium) and library compounds dissolved in DMSO were added to 6.3 μ M final concentration (0.63% final DMSO concentration). After an additional 96 hour incubation at 37 °C, parasite viability was assessed using the BetaGlo Luminiscent Assay (Promega) as described previously³². Compounds causing more than 50% reduction in parasite viability were considered hits. Because of a large number of screen hits, we further followed upon only on a small subset of hits that were also identified as confirmed hits in *L. donovani* and *T. brucei* high throughput screens. Out of 93 such hits, 77 compounds were confirmed to be selective pan-kinetoplastid inhibitors (*L. donovani*, *T. brucei*, *T. cruzi* EC₅₀ values < 10 μ M, selectivity index relative to 3T3 CC₅₀ > 5).

3. Chemical synthesis

Unless otherwise noted, materials were obtained from commercial suppliers and were used without purification. Removal of solvent under reduced pressure refers to distillation using Büchi rotary evaporator attached to a vacuum pump (~3 mm Hg). Products obtained as solids or high boiling oils were dried under vacuum (~1 mm Hg). Purification of compounds by high pressure liquid chromatography was achieved using a Waters 2487 series with Ultra 120 5 μ m C18Q column with a linear gradient from 10% solvent A (acetonitrile with 0.035% trifluoroacetic acid) in solvent B (water with 0.05% trifluoroacetic acid) to 90% A in four minutes, followed by two and half minute elution with 90% A.

¹H NMR spectra were recorded on Bruker XWIN-NMR (400 MHz or 600 MHz). Proton resonances are reported in parts per million (ppm) downfield from tetramethylsilane (TMS). ¹H NMR data are reported as multiplicity (s - singlet, d - doublet, t - triplet, q - quartet, quint - quintet, sept - septet, dd - doublet of doublets, dt - doublet of triplets, bs - broad singlet), number of protons and coupling constant in Hertz. For spectra obtained in CDCl₃, DMSO-*d*₆, CD₃OD, the residual protons (7.27, 2.50 and 3.31 ppm respectively) were used as the reference.

Analytical thin-layer chromatography (TLC) was performed on commercial silica plates (Merck 60-F 254, 0.25 mm thickness); compounds were visualized by UV light (254 nm). Flash chromatography was performed either by CombiFlash® (Separation system Sg. 100c, ISCO) or using silica gel (Merck Kieselgel 60, 230-400 mesh). Agilent 1100 series liquid chromatograph/ mass selective detector (LC/MSD) was used to monitor the progress of reactions and check the purity of products using 254 nm and 220 nm wavelengths, and electrospray ionization (ESI) positive mode. Mass spectra were obtained in ESI positive mode. Elemental analyses were carried out by Midwest microlabs LLC, Indianapolis.

3.1. Synthesis of GNF5343

GNF5343 is a commercially available compound and was purchased from Chembridge laboratories (catalogue # 5840200).

3.2. Synthesis of GNF6702; N-(4-fluoro-3-(6-(pyridin-2-yl)-[1,2,4]triazolo[1,5-a]pyrimidin-2-yl)phenyl)-2,4-dimethyloxazole-5-carboxamide

3.2.1. Synthesis of 2-fluoro-5-nitrobenzoyl chloride (1)

A solution of 2-fluoro-5-nitrobenzoic acid (50 g, 270 mmol) in thionyl chloride (100 mL) was heated to 80 °C and stirred for 4 hours. The mixture was allowed to cool down to room temperature and the solvent was removed to give compound **1** (54 g, 98% yield).

3.2.2. Synthesis of 2-(2-fluoro-5-nitrobenzoyl)hydrazine-1-carboximidamide (2)

To a solution of aminoguanidine carbonate (36.2 g, 266 mmol) in dry toluene (300 mL) at 0 °C, was added compound **1** (54 g, 0.266 mol) over 30 minutes. The mixture was stirred at room temperature for 12 hours. The formed precipitate was removed by filtration, and the residue was treated with H₂O (400 mL) and made alkaline with sodium carbonate. The solid was collected and recrystallized from water to obtain compound **2** (62 g, 97% yield). M/Z 241.1 (M+1).

3.2.3. Synthesis of 5-(2-fluoro-5-nitrophenyl)-4H-1,2,4-triazol-3-amine (**3**)

A solution of compound **2** (62 g, 0.257 mol) in H₂O (800 mL) was stirred for 8 hours at 100 °C. After cooling, the obtained solid was filtered, and the cake was washed with H₂O (100 mL), tetrahydrofuran (100 mL), and dried to give compound **3** (34 g, 51% yield). ¹H NMR (400 MHz, DMSO) 12.42 (s, 1H), 8.74 (dd, *J* = 6.27, 3.01, 1H), 8.26 (dt, *J* = 8.97, 3.42, 1H), 7.57 (t, *J* = 9.54, 1H), 6.29 (s, 2H).

3.2.4. Synthesis of 2-(2-fluoro-5-nitrophenyl)-6-(pyridin-2-yl)-[1,2,4]triazolo[1,5-a] pyrimidine (**4**)

To a solution of compound **3** (1 g, 4.48 mmol) in acetic acid (20 mL) 2-(pyridin-2-yl)malonaldehyde (0.8 g, 5.376 mmol) was added at room temperature. The mixture was heated to 100 °C and stirred for 4 hours. The mixture was allowed to cool to room temperature before adding water (50 mL), filtered, and the filter cake was washed with saturate sodium bicarbonate solution (100 mL), H₂O (100 mL), and tetrahydrofuran (100 mL) and dried under vacuum to give compound **4** (0.9 g, 60% yield). ¹H NMR (400 MHz, DMSO) 10.13 (d, *J* = 2.01, 1H), 9.68 (d, *J* = 2.01, 1H), 9.09- 9.02 (m, 1H), 8.77 (d, *J* = 4.27, 1H), 8.28-8.19 (m, 1H), 8.15-7.96 (m, 2 H), 7.77 (t, *J* = 9.54, 1H), 7.56-7.43 (m, 1H).

3.2.5. Synthesis of 4-fluoro-3-(6-(pyridin-2-yl)-[1,2,4]triazolo[1,5-a]pyrimidin-2-yl)aniline (**5**)

To a solution of compound **4** (0.15 g, 0.443 mmol) in tetrahydrofuran (5 mL) was added Raney Nickel (0.2 g) and ZnI₂ (71 mg) at room temperature. The mixture was stirred under H₂ (50 psi) at 25 °C for 2.5 hours. The mixture was diluted with methanol (10 mL) and filtered. The solvent was removed and the crude product was washed with methanol (5 mL x 2) and dried under vacuum to give compound **5** (90

1046 mg, 66% yield). ¹H NMR (400 MHz, DMSO) 10.01-10.06 (m, 1H), 9.62-9.58 (m, 1H), 8.73-8.78 (m,
1047 1H), 8.24-8.20 (m, 1H), 8.02-7.96 (m, 1H), 7.57-7.47 (m, 2H), 7.08-7.05 (m, 1H), 6.76-6.70 (m, 1H),
1048 5.24 (s, 2H) M/Z 307.01 (M+1).

1049 **3.2.6. Synthesis of N-(4-fluoro-3-(6-(pyridin-2-yl)-[1,2,4]triazolo[1,5-a]pyrimidin-2-yl)phenyl)-2,4-**
1050 **dimethyloxazole-5-carboxamide (GNF6702; 6)**

1051 To a solution of 2,4-dimethyloxazole-5-carboxylic acid (40.6 mg, 0.28 mmol) in dimethylformamide (5
1052 mL) was added HATU (118.6 mg, 0.31 mmol) and DIEA (72.4 mg, 0.56 mmol) at room temperature.
1053 The mixture was stirred for 30 min, the intermediate **5** (80 mg, 0.26 mmol) was added at room
1054 temperature. The mixture was stirred for 3 hours, water (10 mL) was added, the mixture was filtered, and
1055 the filter cake was washed with H₂O (5 mL x 2), tetrahydrofuran (5 mL x 2) and purified by HPLC to
1056 give product **6** (33 mg, 31% yield). ¹H NMR (400 M, MeOD) 9.84 (d, *J* = 2.4, 1H), 9.61 (d, *J* = 2.3, 1H),
1057 8.76 (dt, *J* = 4.8, 1.4, 1H), 8.54 (dd, *J* = 6.4, 2.7, 1H), 8.12 (dt, *J* = 8.0, 1.1, 1H), 8.00 (td, *J* = 7.8, 1.8,
1058 1H), 7.93 (ddd, *J* = 8.9, 4.1, 2.7, 1H), 7.49 (ddd, *J* = 7.5, 4.9, 1.0, 1H), 7.34 (dd, *J* = 10.4, 9.0, 1H), 2.57
1059 (s, 3H), 2.48 (s, 3H). M/Z= 430.13 (M+1).

1060 **3.3. Synthesis of GNF3943; Isopropyl (2-(2-chloro-5-(furan-2-carboxamido)phenyl)-1H-**
1061 **imidazo[4,5-b]pyridin-6-yl)carbamate**

1062 **3.3.1. Synthesis of 2-chloro-5-(furan-2-carboxamido)benzoic acid (7)**

1063 To a suspension of 5-amino-2-chlorobenzoic acid (13.7 g, 79.85 mmol, 1.00 equiv) in tetrahydrofuran
1064 (100 mL) was added furan-2-carbonyl chloride (11.5 g, 88.10 mmol, 1.10 equiv) at 0 °C. The ice bath
1065 was then removed and the reaction was stirred overnight at room temperature. The resulting mixture was
1066 concentrated under vacuum and diluted with DCM. The solid was collected by filtration to give 17 g
1067 (80%) of 2-chloro-5-(furan-2-amido)benzoic acid (**7**) as a gray solid.

3.3.2. Synthesis of *N*-(4-chloro-3-[6-nitro-1*H*-imidazo[4,5-*b*]pyridin-2-yl]phenyl)furan-2-carboxamide (8)

A mixture of 5-nitropyridine-2,3-diamine (6 g, 38.93 mmol, 1.00 equiv) and 2-chloro-5-(furan-2-amido)benzoic acid (**7**) (10.4 g, 39.15 mmol, 1.00 equiv) in polyphosphoric acid (PPA) (100 mL) was stirred overnight at 130 °C. The reaction was then poured into water/ice and the pH value of the mixture was adjusted to 9 with sodium carbonate. The solids were collected by filtration and applied onto a silica gel column with ethyl acetate/petroleum ether (3/1) to give 3.9 g (26%) of *N*-(4-chloro-3-[6-nitro-1*H*-imidazo[4,5-*b*]pyridin-2-yl]phenyl)furan-2-carboxamide (**8**) as a light yellow solid. ¹H NMR (400 MHz, DMSO) δ 10.50 (s, 1H), 9.19 (d, *J* = 2.6 Hz, 1H), 8.73 (s, 1H), 8.43 (d, *J* = 2.6 Hz, 1H), 8.03 – 7.90 (m, 4H), 7.61 (d, *J* = 8.9 Hz, 1H), 7.41 (d, *J* = 3.6 Hz, 1H), 6.79 – 6.67 (m, 1H). MS *m/z* 383.9 (M+H)⁺.

3.3.3. Synthesis *N*-(3-[6-amino-1*H*-imidazo[4,5-*b*]pyridin-2-yl]-4-chlorophenyl)furan-2-carboxamide (9)

To a suspension of *N*-(4-chloro-3-[6-nitro-1*H*-imidazo[4,5-*b*]pyridin-2-yl]phenyl)furan-2-carboxamide (3.9 g, 10.16 mmol, 1.00 equiv) in ethanol (50 mL) was added SnCl₂·2H₂O (3.4 g, 15.04 mmol, 1.48 equiv) and the resulting mixture was heated to reflux overnight. The reaction mixture was concentrated under vacuum and diluted with H₂O. The pH value of the mixture was adjusted to 9 with saturated sodium carbonate. The solids were collected by filtration and applied onto a silica gel column with ethyl acetate/PE (3/1) to give 1.95 g (54%) of *N*-(3-[6-amino-1*H*-imidazo[4,5-*b*]pyridin-2-yl]-4-chlorophenyl)furan-2-carboxamide (**9**) as a yellow solid. ¹H-NMR: (CD₃OD, 400 MHz): 8.16 (d, *J* = 2.4 Hz, 1H), 7.97-8.10 (m, 2H), 7.78 (d, *J* = 0.8 Hz, 1H), 7.65 (d, *J* = 20.0 Hz, 1H), 7.31-7.41 (m, 2H), 6.68 (dd, *J* = 3.6, 2.0 Hz, 1H). MS (M+H)⁺=354.

3.3.4. Synthesis of Isopropyl (2-(2-chloro-5-(furan-2-carboxamido)phenyl)-1*H*-imidazo[4,5-*b*]pyridin-6-yl)carbamate (GNF3943) (10)

To a 20 mL vial was transferred N-(3-(6-amino-1H-imidazo[4,5-b]pyridin-2-yl)-4-chlorophenyl)furan-2-carboxamide **9** (80 mg, 0.225 mmol) in dimethylformamide (4 mL) followed by addition of pyridine (2 drops), and the reaction mixture was stirred at 0 °C for 10 minutes. At this point was added isopropyl carbonochloridate (1 M solution in toluene, 1.45 mmols, 6.4 eq). The reaction mixture was stirred overnight while slowly warming up to room temperature. The presence of desired peak (M+H (440)) was confirmed by LC/MS. The reaction mixture was then quenched with saturated sodium carbonate solution to neutralize the extra acid chloride and to make the solution basic (pH 8-9). The reaction was extracted with ethyl acetate (3x10 mL), and the resulting organics were dried over sodium sulfate, filtered, and dried under vacuum. The resulting residue was purified via ISCO column chromatography using (0-100% ethyl acetate/hexane) to provide 53 mg, 0.119 mmol, 53% of the desired compound. ¹H NMR (400 MHz, MeOD) δ 8.28 (d, *J* = 22.1, 2H), 8.10 (s, 1H), 7.88 (s, 1H), 7.67 (d, *J* = 1.0, 1H), 7.51 (d, *J* = 8.8, 1H), 7.24 – 7.16 (m, 1H), 6.56 (dd, *J* = 1.7, 3.5, 1H), 4.91 (dt, *J* = 6.2, 12.5, 1H), 1.24 (d, *J* = 6.2, 6H). M/Z=440.1(M+1)

3.4. Synthesis of GNF8000; isopropyl (2-(2-fluoro-5-(furan-2-carboxamido)phenyl) imidazo[1,2-a]pyrimidin-6-yl)carbamate

3.4.1. Synthesis of 1-(2-fluoro-5-nitrophenyl)ethan-1-one (11)

A 3,000 mL three necked flask equipped with a mechanic stirrer was charged with concentrated H₂SO₄ (720 mL) and cooled to -40 °C. 1-(2-fluorophenyl)ethanone (180 g, 1.3 mol) was added, followed by addition of a mixture of fuming HNO₃ (106.2 mL) in concentrated H₂SO₄ (260 mL) dropwise over 45 minutes. This mixture was stirred at this temperature for 15 minutes, poured into ice (8 kg), and extracted with ethyl acetate (2000 mL x 2). The combined ethyl acetate layer was washed with saturated NaHCO₃ solution (800 mL x 3), brine (800 mL), dried with anhydrous sodium sulfate, and concentrated under vacuum. The residue was crystallized with petroleum ether to give compound **11** (200 g, yield: 84%) as a

1114 yellow solid. ¹H NMR (400 MHz, CDCl₃) δ 7.34 (t, *J* = 9.29 Hz, 1H), 8.33-8.48 (m, 1H), 8.78 (dd, *J* =
1115 6.15, 2.89 Hz, 1H).

1116 **3.4.2. Synthesis of 2-bromo-1-(2-fluoro-5-nitrophenyl)ethan-1-one (12)**

1117 To a solution of compound **11** (126 g, 0.688 mol) in acetic acid (860 mL) and 40% HBr solution (825.6
1118 mL) at 0 °C, was added a solution of Br₂ (110 g, 0.688 mol) in acetic acid (344 mL) in one portion. This
1119 mixture was stirred at room temperature overnight, diluted with water (3000 mL), and extracted with 50%
1120 ethyl acetate/petroleum ether (1500 mL x 2). The combined organic layer was washed with a saturated
1121 NaHCO₃ solution (1000 mL x 2), brine (1000 mL), dried with anhydrous sodium sulfate and
1122 concentrated. The residue was purified by column chromatography on silica gel (20% EA/PE) to give the
1123 compound **12** (150 g, yield: 83%) as a white solid. ¹H NMR (400 MHz, CDCl₃) δ 8.85 (dd, *J* = 5.90, 2.89
1124 Hz, 1H), 8.42-8.58 (m, 1H), 7.42 (t, *J* = 9.29 Hz, 1H), 4.52 (d, *J* = 2.01 Hz, 2H).

1125 **3.4.3. Synthesis of Isopropyl (2-aminopyrimidin-5-yl)carbamate (13)**

1126 A suspension of 5-nitropyrimidine-2-amine (1 eq.) and Pd/C (0.05 eq.) in ethanol (0.1 mM) was stirred
1127 under hydrogen atmosphere overnight at room temperature to give of 2,5-diaminopyrimidine. The
1128 mixture was then filtered and concentrated under vacuum. The residue (1 eq.) was subjected to coupling
1129 with isopropylcarbonochloridate (1.5 eq.) in anhydrous pyridine (0.3 mM) overnight at room temperature.
1130 The mixture was concentrated under vacuum, and the residue was extracted with ethyl acetate, washed
1131 with brine, dried over anhydrous MgSO₄ (s), filtered and concentrated under vacuum to give **13** as a
1132 yellow solid. *m/z* (ESI): 196 (M + H⁺).

1133 **3.4.4. Synthesis of isopropyl (2-(2-fluoro-5-nitrophenyl)imidazo[1,2-a]pyrimidin-6-yl)carbamate** 1134 **(14)**

1135 Into a 500 mL round-bottom flask, was placed 2-bromo-1-(2-fluoro-5-nitrophenyl)ethan-1-one **12** (30 g,
1136 114.49 mmol, 1 eq.), propan-2-yl N-(2-aminopyrimidin-5-yl)carbamate (11.2 g, 57.08 mmol, 0.5 eq.) and

1137 acetone (200 mL). The resulting solution was stirred overnight at 70 °C. The reaction mixture was cooled
1138 down and the solids were collected by filtration resulting in 15 g (36%) of propan-2-yl N-[2-(2-fluoro-5-
1139 nitrophenyl)imidazo[1,2-a]pyrimidin-6-yl]carbamate (**14**) as a brown solid.

1140 **3.4.5. Synthesis of isopropyl (2-(5-amino-2-fluorophenyl)imidazo[1,2-a]pyrimidin-6-yl)carbamate**
1141 **(15)**

1142 Into a 1 L round-bottom flask was placed tetrahydrofuran (500 mL), Raney Ni (15 g) and propan-2-yl N-
1143 [2-(2-fluoro-5-nitrophenyl)imidazo[1,2-a]pyrimidin-6-yl]carbamate **14** (8 g, 22.26 mmol, 1 eq.). The
1144 resulting solution was stirred overnight at room temperature under an atmosphere of hydrogen. The solids
1145 were filtered out, and washed with methanol (200 mL x 4). The resulting mixture was concentrated under
1146 vacuum to give 7 g (95%) of propan-2-yl N-[2-(5-amino-2-fluorophenyl)imidazo[1,2-a]pyrimidin-6-
1147 yl]carbamate (**15**) as a brown solid. ¹H NMR (400 MHz, DMSO-*d*₆) δ 9.94 (s, 1H), 9.24 (s, 1H), 8.46-
1148 8.47 (m, 1H), 8.26-8.28 (m, 1H), 7.51-7.53 (m, 1H), 6.96-7.02 (m, 1H), 6.55-6.59 (m, 1H), 4.89-4.98 (m,
1149 1H), 3.17 (s, 2H), 1.07-1.30(m, 6H). MS *m/z*= 330 (M+1).

1150 **3.4.6. Synthesis of isopropyl (2-(2-fluoro-5-(furan-2-carboxamido)phenyl) imidazo[1,2-a]pyrimidin-**
1151 **6-yl)carbamate (GNF8000) (16)**

1152 In a 40 mL vial, pyridine (10 mL) was added to intermediate **15** (0.5 g, 1.518 mmol) to give a yellow
1153 solution. To this solution was added furan-2-carbonyl chloride (0.198 g, 1.518 mmol) at 0 °C and the
1154 resulting mixture was stirred for 1 hour. The reaction mixture was quenched with 60 mL of water and
1155 extracted with ethyl acetate. The same step was repeated once more time to remove any extra pyridine.
1156 All organic phases were combined, dried over sodium sulfate and purified by flash chromatography to
1157 give product **16** (ethyl acetate/methanol= 0-10%). ¹H NMR (400 MHz, DMSO-*d*₆) δ 10.43 (s, 1H), 10.06
1158 (s, 1H), 9.36 (s, 1H), 8.69 (dd, *J* = 2.8, 6.9 Hz, 1H), 8.56 (d, *J* = 2.7 Hz, 1H), 8.45 (d, *J* = 4.2 Hz, 1H),
1159 8.02 (d, *J* = 1.0 Hz, 1H), 7.95-7.85 (m, 1H), 7.46 (d, *J* = 3.4 Hz, 1H), 7.37 (dd, *J* = 9.0, 10.9 Hz, 1H),

1160 6.78 (dd, $J = 1.7, 3.5$ Hz, 1H), 5.00 (dt, $J = 6.3, 12.5$ Hz, 1H), 1.35 (d, $J = 6.2$ Hz, 6H). MS $m/z = 424$
1161 (M+1).

1162 **3.5. Synthesis of GNF3849; N-(4-fluoro-3-(6-phenyl-[1,2,4]triazolo[1,5-a]pyrimidin-2-yl)phenyl)-**
1163 **2,4-dimethyloxazole-5-carboxamide**

1164 **3.5.1. Synthesis of 2-(2-fluoro-5-nitrophenyl)-6-phenyl-[1,2,4]triazolo[1,5-a]pyrimidine (17)**

1165 To a solution of compound **3** (0.5 g, 2.24 mmol) in AcOH (5 mL) was added 2-phenylmalonaldehyde
1166 (0.39 g, 2.7 mmol). The mixture was then heated to 100 °C and stirred for 4 hours. The mixture was
1167 allowed to cool to room temperature, water (10 mL) was added, the solids filtered, and the filter cake was
1168 washed with tetrahydrofuran, and dried under vacuum to give compound **17** (0.36 g, 48% yield). ^1H
1169 NMR (400 MHz, DMSO) 9.93 (d, $J = 2.4$, 1H), 9.38 (d, $J = 2.8$, 1H), 8.90 (s, 1H), 7.93 (d, $J = 7.78$, 2H),
1170 7.69 (d, $J = 8.53$, 1H), 7.61-7.50 (m, 2H), 7.31 (t, $J = 7.40$, 1H), 6.88 (s, 1H).

1171 **3.5.2. Synthesis of 4-fluoro-3-(6-phenyl-[1,2,4]triazolo[1,5-a]pyrimidin-2-yl)aniline (18)**

1172 To a solution of compound **17** (2.5 g, 7.4 mmol) in tetrahydrofuran (200 mL) was added ZnI_2 (1.2 g, 3.7
1173 mmol) and Raney Nickel (3.5 g). This mixture was stirred at room temperature for 4 hour under H_2 at 50
1174 psi, then the mixture was filtrated and washed with methanol (20 mL) to give compound **18** (2.0 g, 87%
1175 yield). ^1H NMR (400 MHz, DMSO) 9.81 (d, $J = 2.4$, 1H), 9.27 (d, $J = 2.8$, 1H), 7.90 (d, $J = 7.6$, 2H),
1176 7.58-7.53 (m, 2H), 7.45-7.50 (m, 2H), 7.09-7.05 (m, 1H), 6.74-6.70 (m, 1H), 5.22 (s, 2H). M/Z 306.1
1177 (M+H $^+$).

1178 **3.5.3. Synthesis of N-(4-fluoro-3-(6-phenyl-[1,2,4]triazolo[1,5-a]pyrimidin-2-yl)phenyl)-2,4-**
1179 **dimethyloxazole-5-carboxamide (GNF3849) (19)**

1180 To a solution of 2,4-dimethyloxazole-5-carboxylic acid (0.56 g, 3.9 mmol) in dimethylformamide (30 mL)
1181 was added DIEA (0.85 g, 6.66 mmol) and HATU (1.5 g, 3.9 mmol). This mixture was stirred at room
1182 temperature for 30 minutes, then compound **18** (1.0 g, 3.28 mmol) was added. The mixture was then

1183 stirred at room temperature for 4 hours, diluted with water (50 mL) and extracted with tetrahydrofuran/
1184 ethyl acetate (100 mL /50 mL), the organic layer was dried over sodium sulfate and concentrated to give
1185 the crude product. It was purified by HPLC to give product **19** (0.91 g, yield, 65%) as a white solid. ¹H
1186 NMR (400 MHz, MeOD) 9.49 (d, *J* = 2.4, 1H), 9.22 (d, *J* = 2.4, 1H), 8.51 (dd, *J* = 6.4, 2.8, 1H), 7.90
1187 (ddd, *J* = 8.9, 4.2, 2.8, 1H), 7.86-7.76 (m, 2H), 7.63-7.55 (m, 2H), 7.54-7.45 (m, 1H), 7.32 (dd, *J* = 10.4,
1188 9.0, 1H), 2.56 (s, 3H), 2.47 (s, 3H). *M/Z*= 429.2 (*M*+*H*⁺).

1189 **3.6. Synthesis of GNF2636; isopropyl (2-(2-chloro-5-(furan-2-carboxamido)phenyl)imidazo[1,2-**
1190 **a]pyrimidin-6-yl)carbamate**

1191 **3.6.1. Synthesis of isopropyl (2-(2-chloro-5-nitrophenyl)imidazo[1,2-a]pyrimidin-6-yl)carbamate**
1192 **(20)**

1193 Into a 500-mL round-bottom flask, was placed **13** (1.75 g, 6.3 mmol, 1.2 equiv), acetone (400 mL) and 2-
1194 bromo-1-(2-chloro-5-nitrophenyl)ethan-1-one (1.0 g, 5.3 mmol). The resulting solution was stirred
1195 overnight at 70 °C. The reaction mixture was cooled, the solvent evaporated, the resulting material
1196 suspended in methanol, and then solids collected by filtration resulting in product **20** (0.75 g, 38% yield).
1197 ¹H NMR (400 MHz, DMSO-*D*₆) δ 10.08 (s, 1H), 9.34 (s, 1H), 9.08 (s, 1H), 8.86 (s, 1H), 8.56 (s, 1H),
1198 8.19 (d, *J* = 8.7, 1H), 7.88 (d, *J* = 8.8, 1H), 4.95 (m, 1H), 1.30 (m, 6H). MS *m/z* (ESI) = 377 (*M* +).

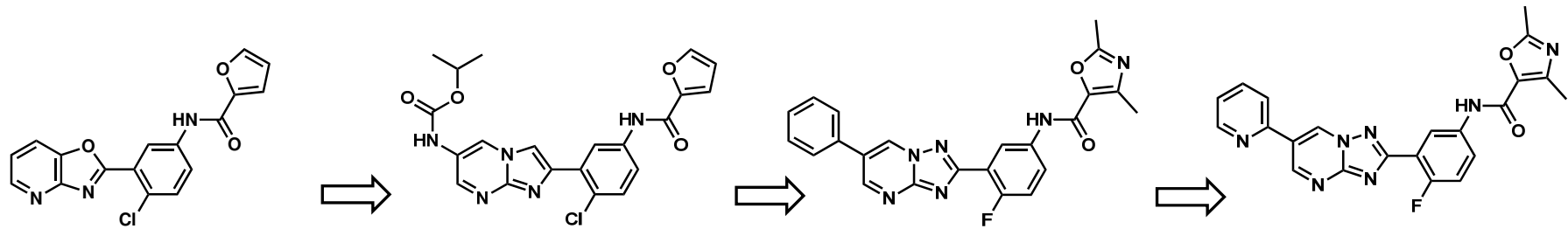
1199 **3.6.2. Synthesis of isopropyl (2-(5-amino-2-chlorophenyl)imidazo[1,2-a]pyrimidin-6-yl)carbamate**
1200 **(21)**

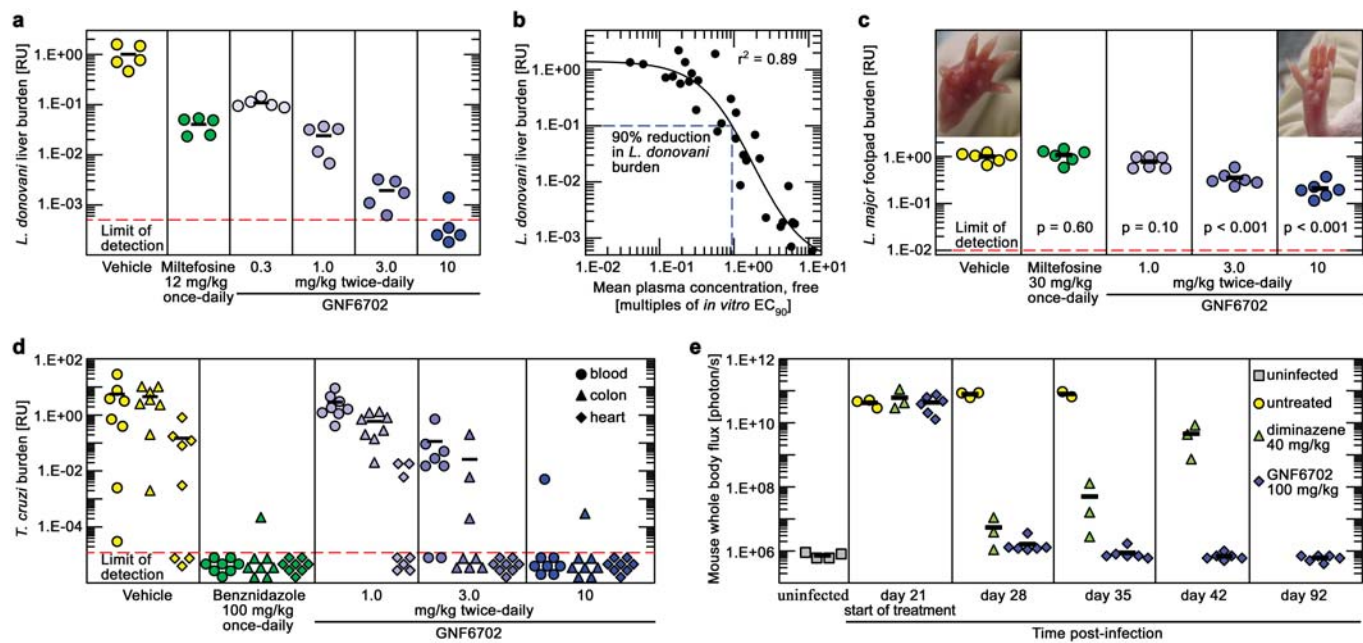
1201 In a round-bottom flask, **20** (300 mg, 0.77 mmol) was taken up in methanol (20 mL) and SnCl₂ (3
1202 equivalents) was added. The resulting mixture was stirred for 2 hours at reflux. The reaction mixture was
1203 concentrated under vacuum and the crude material was purified by flash column chromatography
1204 (hexane/ ethyl acetate solvent system followed by DCM/methanol solvent system) resulting in **21** (265
1205 mg, 96%) as a yellow solid. ¹H-NMR: (300 MHz, MeOD): 9.30 (s, 1H), 8.51 (d, *J* = 2.1 Hz, 1H), 8.37 (s,

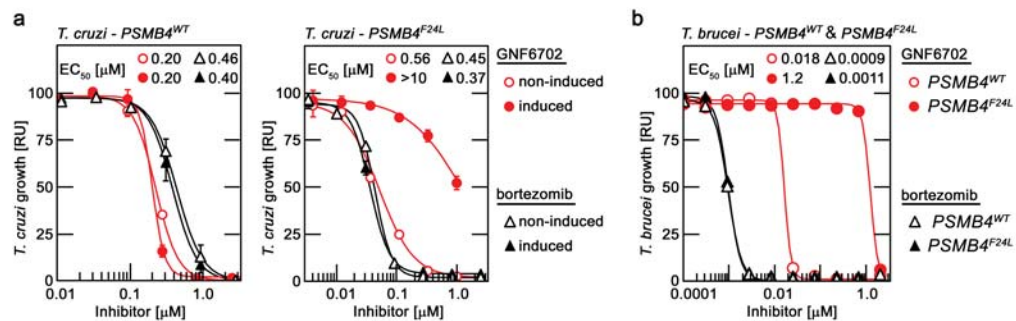
1206 1H), 7.37 (d, $J = 1.8$ Hz, 1H), 7.23 (d, $J = 6.6$ Hz, 1H), 6.72-6.74 (m, 1H), 5.01-5.07 (m, 1H), 1.24-1.36
1207 (m, 6H). MS $m/z = 346$ (M+H+).

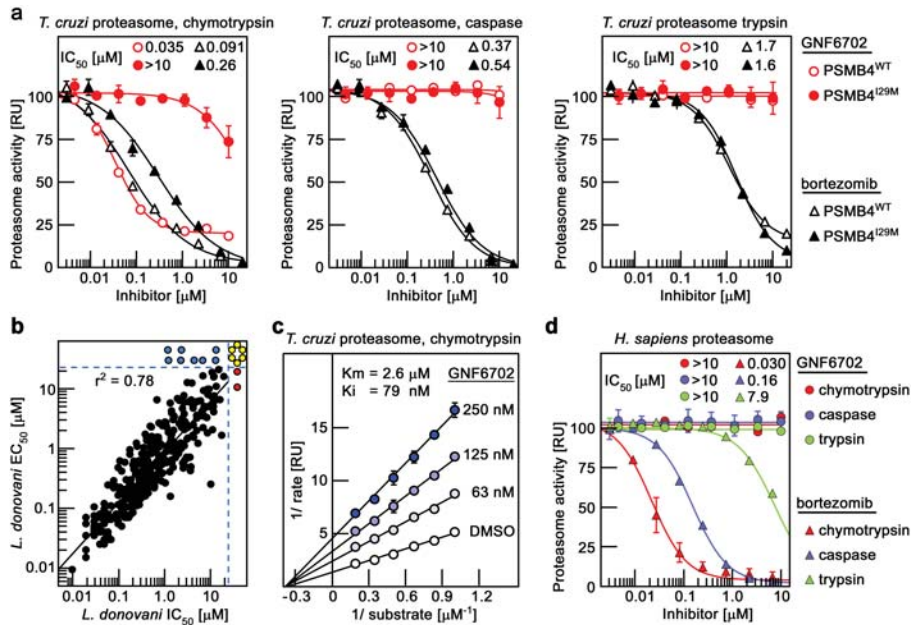
1208 **3.6.3. Synthesis of isopropyl (2-(2-chloro-5-(furan-2-carboxamido)phenyl)imidazo[1,2-a]**
1209 **pyrimidine-6-yl)carbamate (GNF2636) (22)**

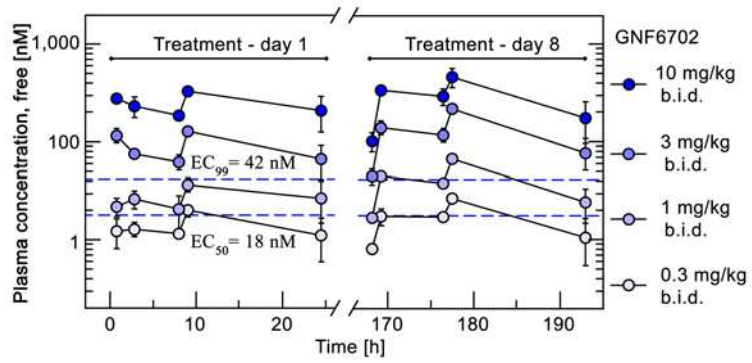
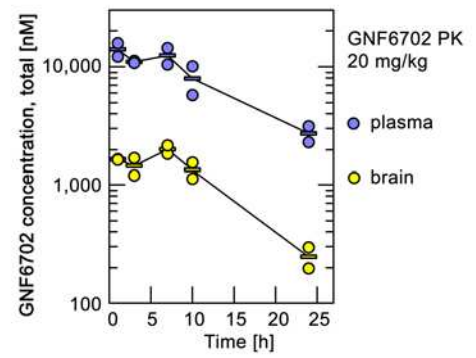
1210 To a suspension of compound **21** (20 mg, 0.06 mmol) in pyridine (2 mL) in a vial was added 2-furoyl
1211 chloride (1.5 equivalents) at room temperature. After stirring overnight, the reaction was concentrated
1212 and the resulting residue was purified by prep HPLC to afford the product **22** (5 mg, 19% yield). ^1H
1213 NMR (400 MHz, methanol- d_4) δ 9.57 (s, 1H), 8.76 (d, $J = 2.6$ Hz, 1H), 8.52 (s, 1H), 8.31 (d, $J = 2.6$ Hz,
1214 1H), 7.89 – 7.69 (m, 2H), 7.62 (d, $J = 8.8$ Hz, 1H), 7.32 (d, $J = 3.5$ Hz, 1H), 6.68 (dd, $J = 3.5, 1.7$ Hz,
1215 1H), 5.14 – 4.97 (m, 1H), 1.35 (d, $J = 6.3$ Hz, 6H). MS $m/z = 440.2$ (M+H).

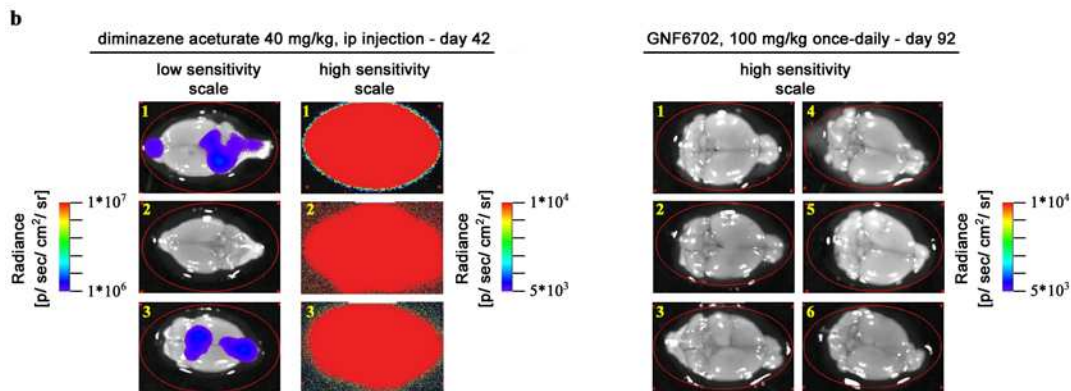
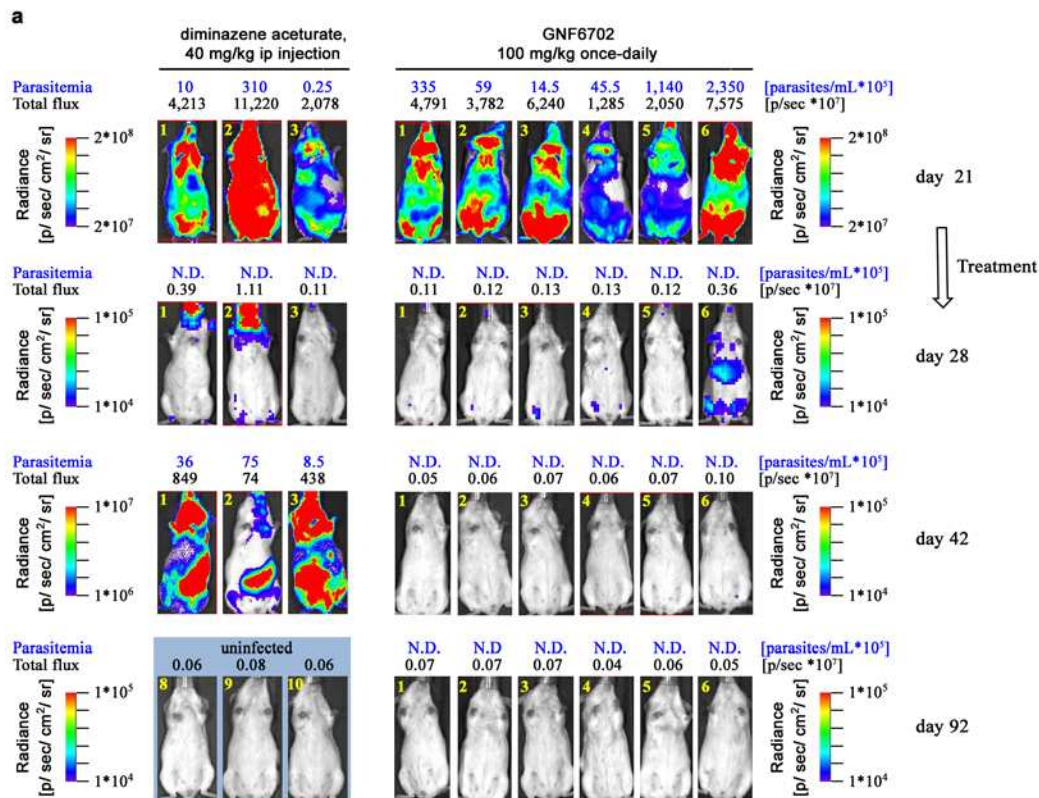


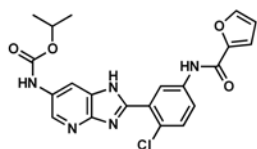






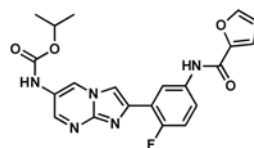
a**b**





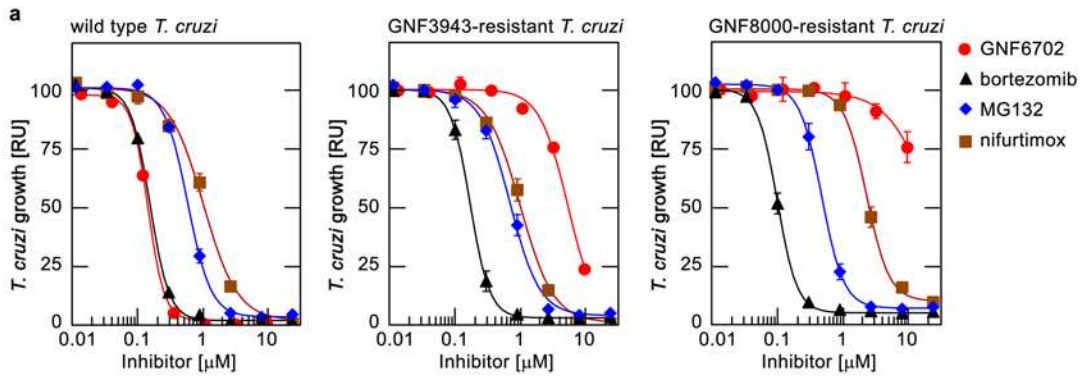
GNF3943

L. donovani EC₅₀ = 380 ± 23 nM
T. brucei EC₅₀ = 33 ± 9.4 nM
T. cruzi EC₅₀ = 120 ± 12 nM
 3T3 CC₅₀ = 4.5 ± 0.9 μM
 Macrophage CC₅₀ = 9.8 ± 2.4 μM
 F = 75 %
 CL = 17.7 mL*min⁻¹*kg⁻¹



GNF8000

L. donovani EC₅₀ = 320 ± 7.1 nM
T. brucei EC₅₀ = 73 ± 2.9 nM
T. cruzi EC₅₀ = 154 ± 12 nM
 3T3 CC₅₀ > 20 μM
 Macrophage CC₅₀ = 18 ± 2.1 μM
 F = 10 %
 CL = 8.8 mL*min⁻¹*kg⁻¹

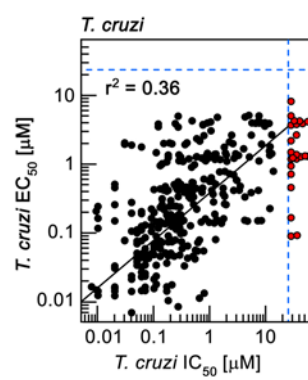
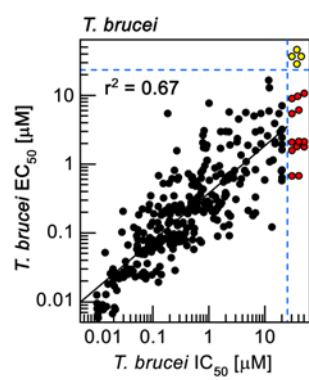


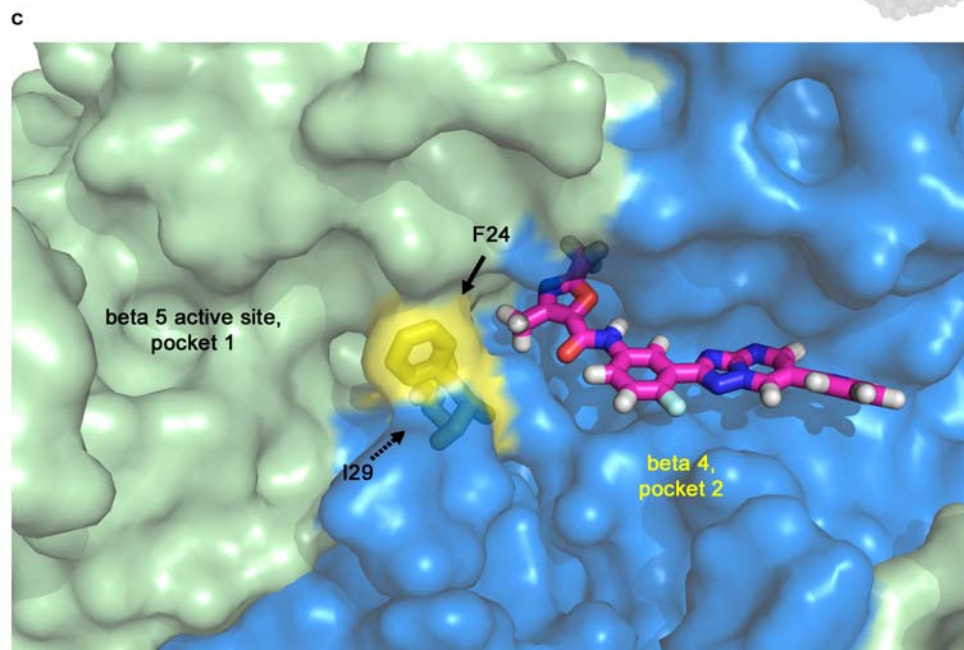
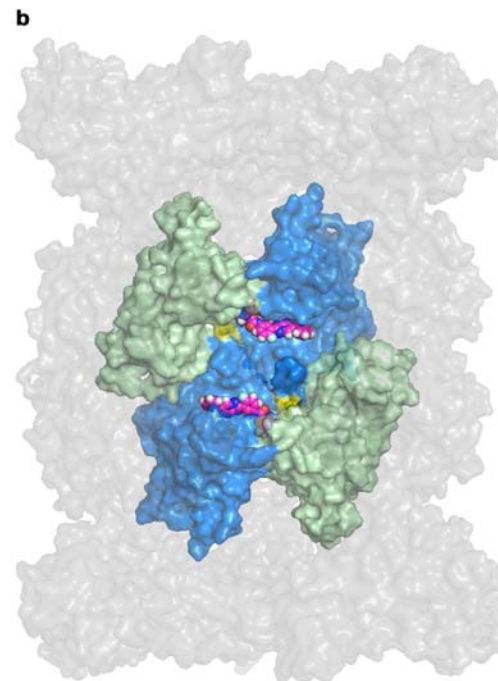
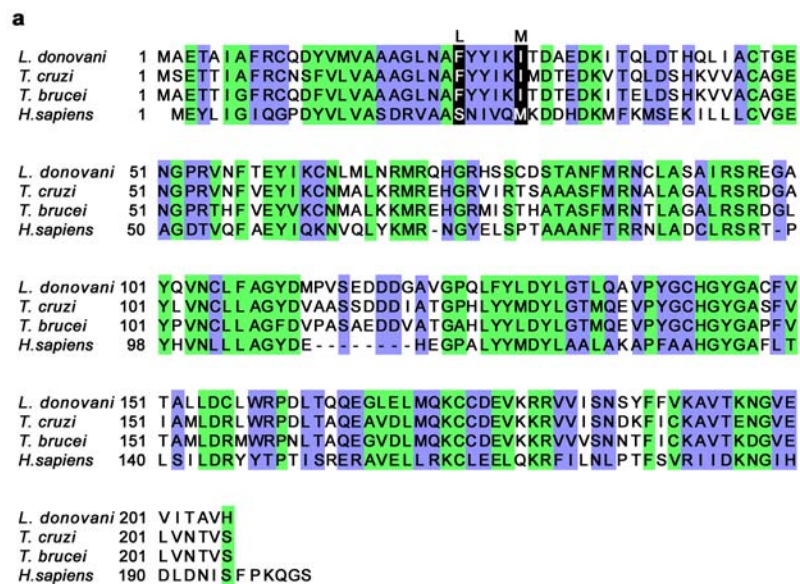
b

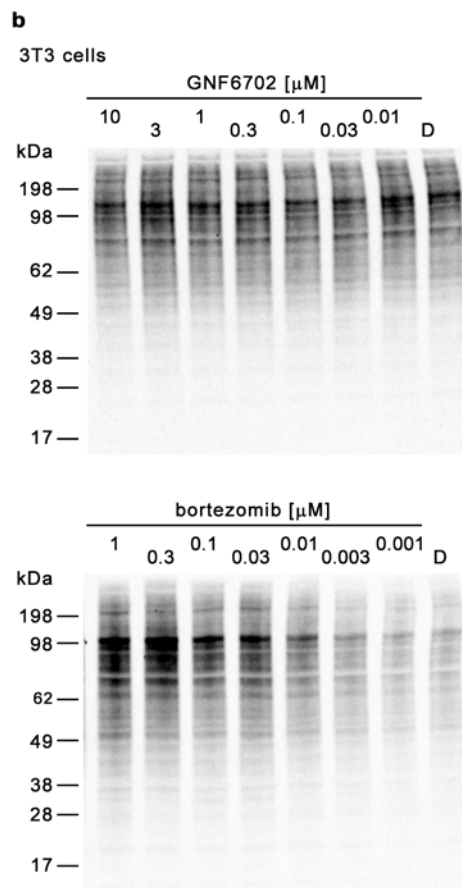
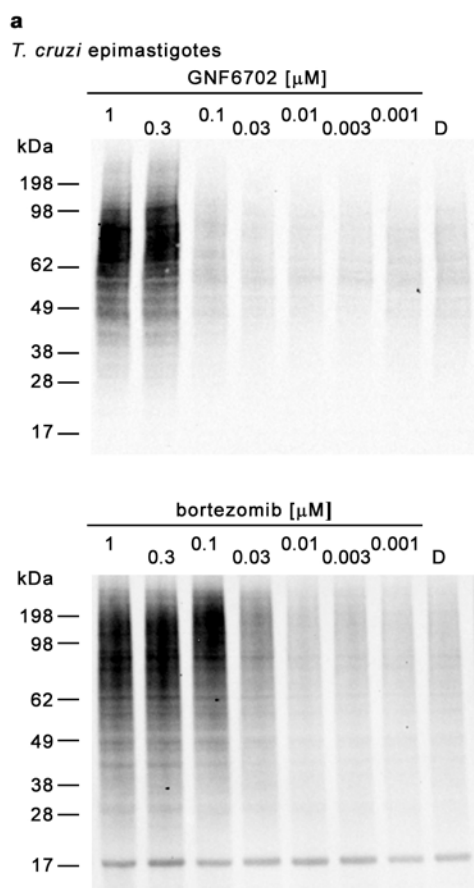
	wt <i>T. cruzi</i>	GNF3943 ^R <i>T. cruzi</i>	GNF8000 ^R <i>T. cruzi</i>
GNF6702 EC ₅₀ [μ M]	0.15 \pm 0.002	5.5 \pm 0.016	> 10
bortezomib EC ₅₀ [μ M]	0.16 \pm 0.006	0.12 \pm 0.020	0.10 \pm 0.007
MG132 EC ₅₀ [μ M]	0.61 \pm 0.015	0.76 \pm 0.071	0.48 \pm 0.052
nifurtimox EC ₅₀ [μ M]	1.0 \pm 0.09	1.0 \pm 0.11	2.4 \pm 0.15

c

		<i>T. cruzi</i> ectopic PSMB4 ^{WT}		<i>T. cruzi</i> ectopic PSMB4 ^{F24L}		<i>T. brucei</i> ectopic PSMB4 ^{WT}		ectopic PSMB4 ^{F24L}
		non-induced	induced	non-induced	induced	constitutive	constitutive	
GNF6702	[μ M]	0.20 \pm 0.007	0.20 \pm 0.023	0.56 \pm 0.029	> 10	0.018 \pm 0.0018	1.2 \pm 0.013	
bortezomib	[μ M]	0.46 \pm 0.059	0.40 \pm 0.057	0.45 \pm 0.008	0.37 \pm 0.015	0.00094 \pm 0.00005	0.0011 \pm 0.00026	





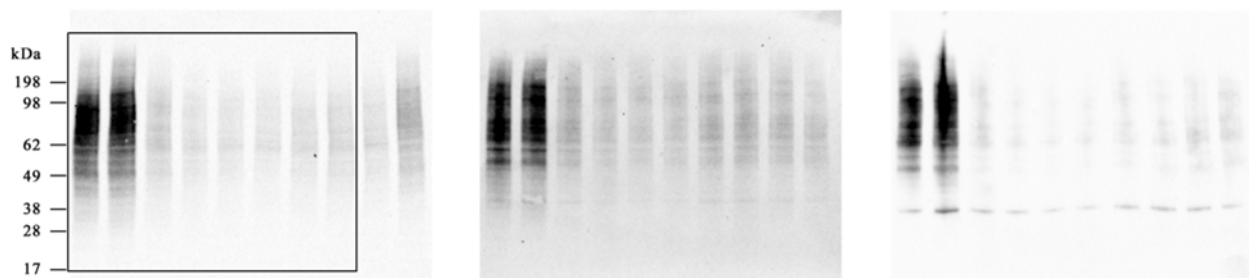


c

		<i>T. cruzi</i>	3T3
GNF6702	EC ₅₀ [μM]	0.13 ± 0.010	> 10
bortezomib	EC ₅₀ [μM]	0.062 ± 0.001	0.040 ± 0.008

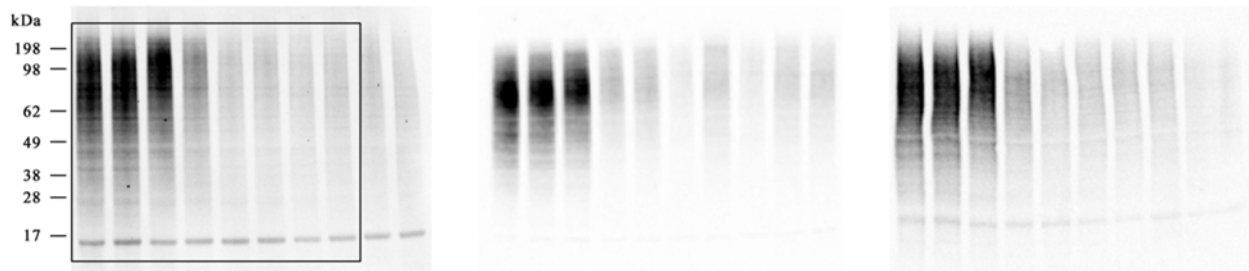
Supplementary Figure 1

a Western blots of three sets of cell lysates from GNF6702-treated *T. cruzi* epimastigotes



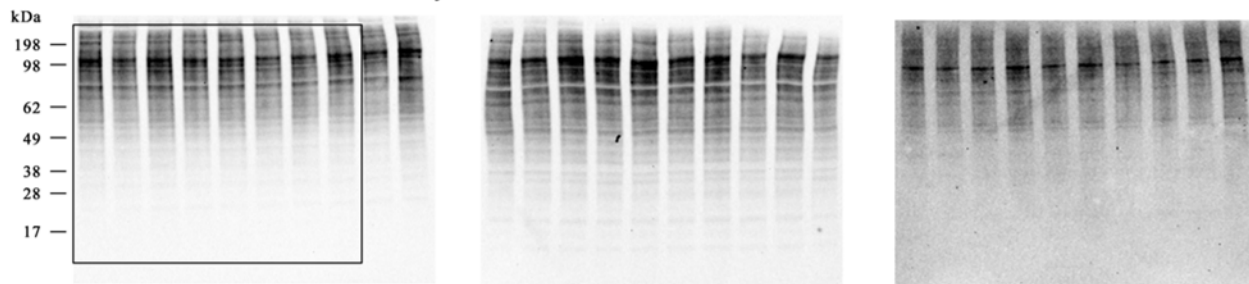
Extended Data Fig. 7a, upper panel

b Western blots of three sets of cell lysates from bortezomib-treated *T. cruzi* epimastigotes



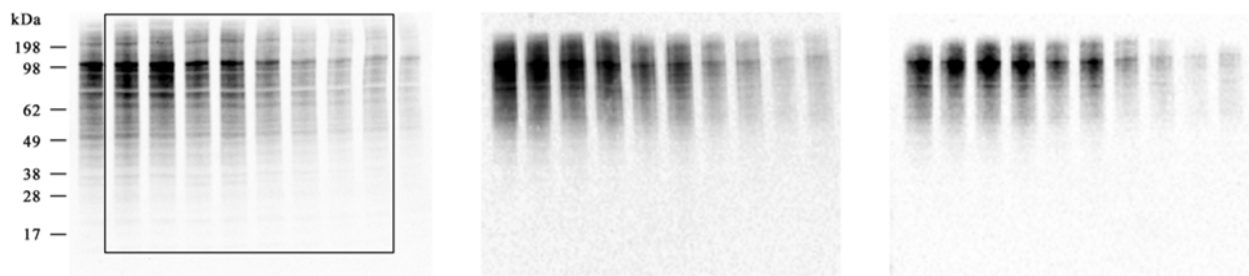
Extended Data Fig. 7a, lower panel

c Western blots of three sets of cell lysates from GNF6702-treated 3T3 cells



Extended Data Fig. 7b, upper panel

d Western blots of three sets of cell lysates from bortezomib-treated 3T3 cells



Extended Data Fig. 7b, lower panel

Excel files

1. [Supplementary Table 1](#)
Small molecule screening data from *Leishmania donovani* axenic amastigote growth inhibition HTS.
2. [Supplementary Table 2](#)
Small molecule screening data from *Trypanosoma brucei* bloodstream form trypomastigote growth inhibition HTS.
3. [Supplementary Table 3](#)
Small molecule screening data from *Trypanosoma cruzi* intracellular trypomastigote growth inhibition HTS.
4. [Supplementary Table 4](#)
Time course of parasitemia in mice infected with bioluminescent *T. brucei* during and after treatment with diminazene aceturate and GNF6702
5. [Supplementary Table 5](#)
Time course of whole body bioluminescence in mice infected with bioluminescent *T. brucei* during and after treatment with diminazene aceturate and GNF6702
6. [Supplementary Table 6](#)
Trypanosoma brucei bioluminescence of *ex vivo* brains obtained from parasite-infected mice after treatment with diminazene aceturate and GNF6702.
7. [Supplementary Table 7](#)
20S proteasome subunits identified in purified *T. cruzi* proteasome.
8. [Supplementary Table 8](#)
Amino acid sequences of predicted *Trypanosoma cruzi* 20S proteasome alpha and beta subunits.
9. [Supplementary Table 9](#)
GNF6702 profile in a panel of mammalian receptors, enzymes and ion channels.
10. [Supplementary Table 10](#)
GNF6702 inhibition profile in a cell-based Ba/F3 panel of Tel-activated human tyrosine kinases.
11. [Supplementary Table 11](#)
GNF6702 ADME profile.